Facultad
de
Ciencias

BÚSQUEDA DE MATERIA OSCURA EN EXPERIMENTOS DE BÚSQUEDA DIRECTA DAMIC
(SEARCH FOR DARK MATTER IN DAMIC DIRECT SEARCH EXPERIMENTS)

Trabajo de Fin de Grado
para acceder al

GRADO EN FÍSICA

Autor: Juan Cortabitarte Gutiérrez

Co-Directora: Rocío Vilar Cortabitarte

Co-Directora: Núria Castelló-Mor

Julio - 2020

Búsqueda de materia oscura en experimentos de búsqueda directa: DAMIC-M
(Search for dark matter in direct search experiments: DAMIC-M)

Resumen

Este trabajo está enmarcado en el **Experimento DAMIC-M** y su prototipo **LBC** (DAMIC-M es un acrónimo para DArk MAtter in CCDs at Modane, mientras que LBC son las siglas para Low Background Chamber). El propósito de DAMIC-M es la búsqueda de partículas de **Materia Oscura** mediante la detección de los retrocesos nucleares y/o de electrones inducidos por Materia Oscura ligera. Una parte crucial para este objetivo es un conocimiento detallado de los ruidos de fondo y la identificación de partículas. La comprensión de estos ha sido el principal objetivo de este trabajo, el cual puede resumirse en: i) validación de **DAMICG4**, una herramienta utilizada para la simulación de las interacciones entre partículas y materia mediante simulaciones Monte Carlo; ii) validación de **psimulCCDimg**, software utilizado para emular la respuesta del detector de DAMIC-M; iii) **creación de una base de datos de partículas simuladas** de diferente naturaleza (principalmente alfas, muones y electrones) que será utilizada en otros dos trabajos dedicados al desarrollo de un algoritmo de machine learning.

Palabras clave: Materia Oscura, CCDs, radiopureza, laboratorio subterráneo, búsqueda directa.

Abstract

The framework of this work is the **DAMIC-M Experiment** and its proof-of-concept **LBC** (DAMIC-M stands for DArk MAtter in CCDs, while LBC for Low-Background Chamber). The purpose of DAMIC-M is search for **Dark Matter** (DM) particles by detecting nuclear or/and electrons recoils induced by light mass Dark Matter. A crucial part of this goal is a detailed knowledge of the backgrounds noise and particle identification. The understanding of this has been the main aim of work in this thesis, which can be summarized as: i) validation of **DAMICG4**, a tool used to simulate the interactions of particles in matter based on Monte Carlo simulations; ii) validation of **psimulCCDimg**, a software used to mimic the response of the DAMIC-M detector; iii) **create a data base of simulated particles** of different nature (mainly alpha, muons and electrons) which are used in other two works focused on machine learning algorithm.

Key words: Dark Matter, CCDs, radiopurity, underground labs, direct searches.

Contents

1 — Introduction

The framework of this work is the **DAMIC-M Experiment** and its proof-of-concept **LBC** (DAMIC-M stands for DArk MAtter in CCDs, while LBC for Low-Background Chamber). The purpose of DAMIC-M is search for **Dark Matter** (DM) particles by detecting nuclear or/and electrons recoils induced by light mass Dark Matter. DAMIC-M is made of **skipper CCDs** (Charge-Coupled Devices forwith skipper readout), the most massive CCDs ever built with exquisite spatial resolution ($15\mu m \times 15\mu m$ pixel). In this novel and unconventional use of CCDs, which are commonly exploded for digital imaging in astronomical telescopes, the DM particle will interact with the atom and the ionization charge will be detected. The crucial innovation in these new CCDs devices is the **skipper technology**, based on a non-destructive, repetitive measurements of the pixel charge, which results in the high-resolution detection of a single electron, this provides an unprecedented sensitivity to light dark matter (eV energies are enough to free and electron in silicon). By counting individual charges in a detector with extremely low leakage current –a combination unmatched by any other DM experiment– DAMIC-M will take a leap forward of several orders of magnitude in the exploration of the hidden sector (see **Section 1.3**), a jump that may be rewarded by serendipitous discovery. A crucial part of this goal is a detailed knowledge of the backgrounds noise and particle identification. The understanding of this has been the main aim of work in this thesis, which can be summarized as: i) validation of **DAMICG4**, a tool used to simulate the interactions of particles in matter based on Monte Carlo simulations (**Section 2.1**); ii) validation of **psimulCCDimg**, a software used to mimic the response of the DAMIC-M detector (**Section 2.2**); and iii) **create a data base of simulated particles** of different nature (mainly alpha, muons and electrons) which are used in other two works focused on machine learning algorithm (Chapter *3*).

1.1 Dark Matter

The search for dark matter is one of the main research lines among the scientific community, and it has astrophysicists, particle physicists and cosmologists working together. Strong evidence is held on the existence of this form of matter that accounts for approximately 85% of matter on the universe and 25% of its total energy density [1].

Dark matter evidence started to ring a bell in the early twentieth century with the measurement of stellar velocities in the Milky Way (Jacobus Kapteyn, 1922, already using the term *dark matter* [2]), but started to get real with the work of Fritz Zwicky in 1933, when he applied the virial theorem to infer the gravitational mass of the to the Coma Cluster, and found evidence that, if verified, "would lead to the surprising result that dark matter exists in much greater density than luminous matter" [3]. By the late 1950s a lot of mass-to-light ratio articles had been published. In 1958, at the eleventh Solvay conference, Viktor Ambartsumian tried to link the dark matter problem to an absence of "dynamical equilibrium" in these clusters, as if their galaxies were flying apart, so

the virial theorem could not be applied and the calculations were misinterpreted. Ambartsumian's idea spread quickly as a viable hypothesis against the unseen matter. The controversy between the two hypotheses lead to the fifteenth symposium of the International Astronomical Union, in Santa Barbara, California. Both ideas seemed problematic. Ambartsumian's was in conflict with the cosmological time scale because the instability would cause the clusters to disappear in 10 to 1000 million years, less than the estimated age of the galaxies compared to the known scale of the universe [4] [5]. On the other hand, the unseen matter hypothesis was "distasteful" for cosmologists and astrophysicists as this implies that "their theories are based on observations of less than 1% of the matter that is really there!" [6]. During the 1960s Kent Ford and Vera Rubin measured the rotation curve of the Andromeda galaxy with quality never seen before thanks to a new image tube spectrograph [7]. This research line lead to new striking evidence on dark matter in 1970 by comparing optical and radio observations on M31 (Andromeda Galaxy, Kent Ford and Vera Rubin), M33 and NGC300 (Ken Freeman). While the optical measurements on galaxies showed a decaying mass distribution from the center, the rotation curves appeared flat, meaning there is some non-visible matter (which density increases towards the outskirts of the galaxy) adding gravitational force. As stated by Ken Freeman [8]: "These data [...] if they are correct, then there must be in these galaxies additional matter which is undetected, either optically or in the radio spectrum. Its mass must be at least as large as the mass of the detected galaxy [...]".

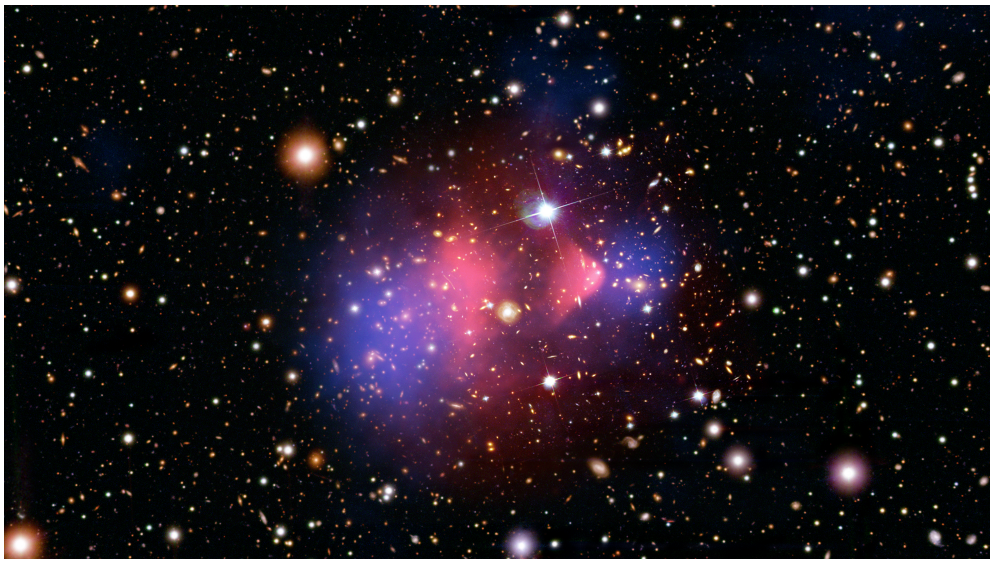

Figure 1.1: Image taken from [9]. This is an image of the Bullet cluster, composed by two galaxy clusters colliding, where the DM escape leaving the normal matter behind. The majority of the "normal" matter in a cluster is the hot gas which slow down in the cluster collision due mainly to electromagnetic interaction that emits X-Rays, shown in pink by X-Ray Chandra survey. On the other hand, using the gravitational lensing technique shows that the lensing does not follow the hot gas, and extend in two areas outside the pink zone coincidence with the visible galaxies shown by the Magellan and the Hubble Space Telescope in the visible range (background). Therefore, the blue zone must be full of non-visible matter, dark matter.

Nowadays, there is overwhelming astrophysical and cosmological evidence for dark matter as a major constituent of the universe (as the example shows in *Figure 1.1*, explanation in the caption). Its gravitational influence is necessary to explain why galaxy clusters are bound together [5] and stars move faster than expected around their galaxy [10], the existence of a large-scale structure in the galaxies distribution in the universe [11] and the features in the Cosmic Microwave power spectrum [12]. Significant efforts have been made to understand the nature of dark matter and theories have been formulated to explain its existence: from modified Newtonian dynamics in the Einstein's General Relativity [13], to Dark Fluid theory [14] but in general terms, we can not talk about dark matter without getting into particle physics, where this work relies.

Conceptually, a new particle(s) was also produced in an early phase of our Universe and interacts (in some "unknown" way) with ordinary matter to dramatically influence the shape of the universe as it is. Many models have appears lately proposing DM candidates with a variate in mass that covers more than 90 orders of magnitude. Much of the DM may be made up of as yet undiscovered particles like WIMPS, SUSY particles, fuzzy dark matter, wave-particles, dark photons, etc. Not only particles, but big objects as primordial black holes, have been proposed.

Here there is a very brief review of the most popular candidates. For instance, **Weakly Interacting Massive Particles** (WIMPs) –the main focus of the vast majority of the direct DM detectors– were produced together with Standard Model (SM) particles in the hot bath of the early universe, ultimately escaping thermal equilibrium. Any of the used techniques (e.g. direct detection, creation in particle accelerators...) have not detected (so far) these hypothetical particles. Axions is another candidate, originally attempts to explain why the strong interaction seems to obey the CP symmetry, but it could be also a candidate to DM. Many experiments search for this particles, or similar called Axion Like PArticles (ALPs).

Another well-motivated alternative is the **Hidden Sector** (HS) particles, proposed by the international community as an alternative approach to go beyond the WIMP paradigm. In this scenario, dark matter is made of particles from one of the many quantum fields that encompasses our entire visible world. For the detection of this particles, whilst the nuclear recoil induced by light dark matter is albeit undetectable, energy transfer in the scattering with electrons or absorption of a dark photon are much more efficient, allowing dark matter direct detection experiments to prove as low as eV.

Unfortunately, no technique (scintillation crystals [15] [16], noble liquids [17] [18] [19], bubble chambers [20], cryogenic calorimeters [21] [22]) has been successful yet in the effort to detect the low-energy recoils or interactions induced by the interactions of these theorized particles. Therefore, its nature, so far elusive, constitutes one of the most exciting mysteries in science.

A sign of dark matter in detectors can be a **direct detection** by observing nuclear recoils from elastic scattering (such as DAMIC [23], XENON [24], DarkSide [25], SuperCDMS [26]), or an annual modulation as a consequence of the Earth rotation around the Sun (e.g. DAMA/LIBRA [15]); or an **Indirect Detection** by searching for the annihilation products of the dark matter being the dark matter self-annihilation cross section the constraining factor (e.g. PAMELA [27], FERMI [28]). The

vast majority of the experiments are optimized to search for WIMPs (XENON, DarkSide, LUX/LZ, SuperCDMS, DAMIC), but there are also searches for other dark matter candidates: axions (e.g. ADMX [29]), SuperWIMPs (e.g. XENON100 [30], XENON1T [19]), graviton (e.g. CMS [31]), hidden sector (e.g. DAMIC-M [32], LDMX [33]), etc. Special attention will be given to direct detection searches where DAMIC-M belongs.

1.2 State of art in direct detection

Direct detection experiments have been running for the last 35 years since, in 1985, Goodman and Witten rethought Drukier and Stodolsky's idea of neutrino detection through elastic scattering with nuclei [34], discussing its usefulness in dark matter particles detection [35]. Stodolsky's general idea was to maintain the detector in a minimal equilibrium, so a very little energy push would make it collapse and create an electrical signal (via superconductors, scintillators, or semiconductors).

As it lays on the interaction with nuclei, it would be possible to find Dark Matter candidates which either can undergo coherent scattering with nuclei, can scatter through spin-dependent couplings or undergo strong interactions (a better explanation in the nuclear physics, and the nuclear recoil process can be found in [36]).

In order to find this little nuclear recoils, DM direct detection experiments need a low energy threshold and a very low background (or at least, to be able to discriminate already known background). This is mandatory to be able to detect the little nuclear recoils, but there is also a need for large detector mass and long term stability, in order to collect as much data as possible at once, reducing exposition time.

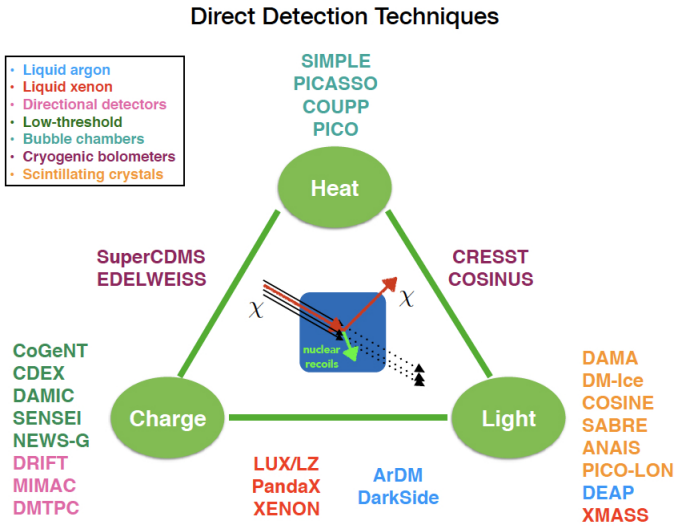

Figure 1.2: Scheme showing different direct detection techniques used for dark matter search and examples of experiments that made use of them.

Different techniques can be used to observe the nuclear recoils (as shown in *Figure 1.2*): either measuring the heat left by the collision (phonon detection via superconductors in cryogenic bolometers like the SuperCDMS), measuring the charge moved by the nuclear recoil (ionization in semiconductors, like DAMIC, or bubble chambers like Sensei [37]) or the light emmited by the detector material (scintillators, like DAMA/LIBRA NaI(Tl) crystalls, or Anais [38]). Some experiments combine two techniques to improve the sensitivity such XENON noble liquid that uses scintillations and ionization or SuperCDMS that uses ionization and heat.

In summary, the best limits on the DM are reached with the noble liquid technique with XENON1T data, the world's most sensitive dark matter experiment (see comparison in *Figure 1.3*), showing a surprising excess of events. The scientists do not claim to have found dark matter. Instead, they say to have observed an unexpected rate of events, the source of which is not yet fully understood. The signature of the excess is similar to what might result from a tiny residual amount of tritium, but could also be a sign of something more exciting.

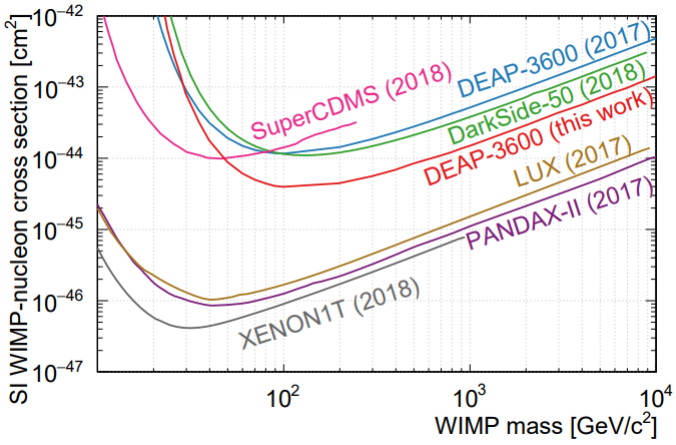

Figure 1.3: Limits on the WIMP-nucleon scattering cross section found by different direct detection experiments. [39]

Independently of the theoretical motivations for any kind of DM, it is important to recognize that current experiments have limited sensitivity to DM-electron interactions, and a light DM particle may have well escaped detection. Most of the interactions result in the production of few charges, requiring the detector to be able to resolve individual electrons. An ubiquitous challenge for DM experiments is also different sources of background (natural radioactivity, airbone radon, neutrons, α particles, neutrinos, etc.) which must be really low for a signal to be recognizable. The sensitivity of Si based detectors is limited by the dark current and understanding of background even in the CCDs itself such as ^{32}Si or $Tritium$. A low dark current is a prerequisite to building a detector to search for light DM using DM-electron interactions.

In this context, innovative technology of a single-electron detection, already demonstrated in CCDs for DAMIC, will enable DAMIC-M to achieve unprecedented sensitivity to the DM hidden

sector. DAMIC-M capitalizes on the DAMIC experience at SNOLAB (next **Section 1.3**) and, at the same time, greatly improves in sensitivity by further innovating the detector technology. In fact, the measurement and mitigation of ^{32}Si and tritium that will be achieved with DAMIC-M are a necessary step to demonstrate the feasibility of a next-generation detector aiming to reach the neutrino floor.

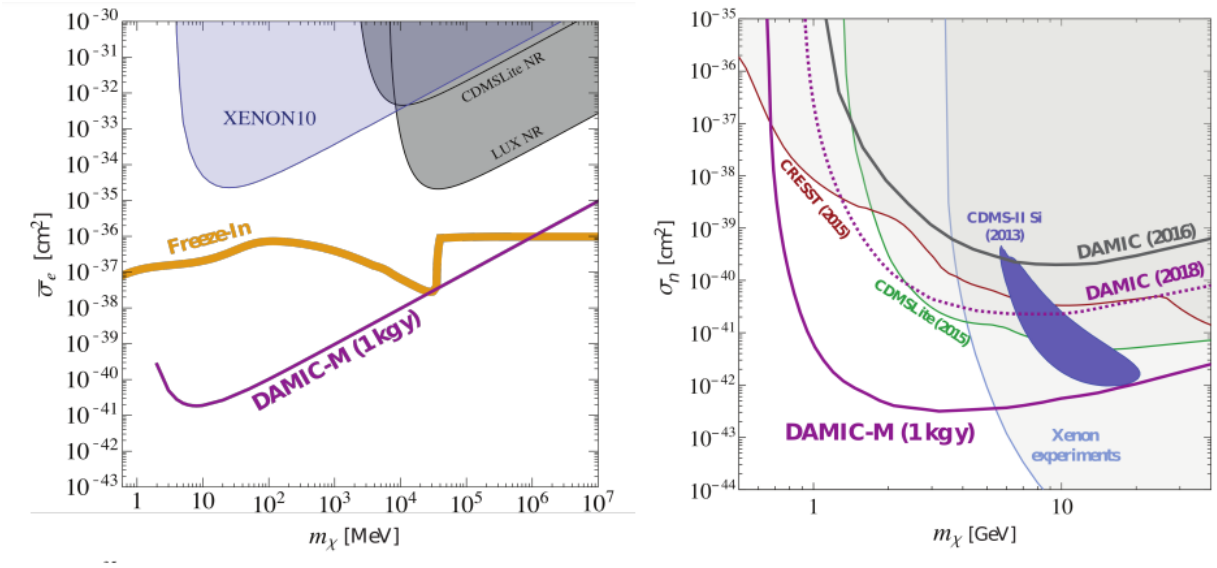

Figure 1.4: DAMIC-M expected sensitivity for Dark Matter-electron for a light hidden photon mediator (left) and WIMP-nucleon spin-independent scattering (right). Exclusion limits from other dark matter searches are shown for comparison. [32]

1.3 DAMIC and the use of CCDs as a Dark Matter detector

As already mentioned, the scope of this work is the upcoming DAMIC-M Experiment, the upgrade of DAMIC. DAMIC use CCDs (charged coupled devices) made of silicon to find signals in the detectors different from the noise when interacting with Si atoms. For that, DAMIC approach is simulating all possible background noise and compare it to the experimental data, if any discrepancy is found, it can be studied and focused to see whether it is Dark Matter, some unpredicted background noise or something else unknown.

CCDs have been previously used in astronomical imaging and spectroscopy, achieving readout noise below 2 e^-, around 7.3 eV of ionizing energy in silicon. The original CCDs comes from the Dark Energy Survey (DES) [40] [41] which used a 250 μm thick CCD to study near-infrared light from astrophysical objects.

DAMIC Experiment

DAMIC Experiment was installed at SNOLAB underground laboratory (at 2000 meters deep). The DAMIC detector employed 7 CCDs of 40 gr, with 4000×4000 pixels of size of 15 μm x 15 μm and 675 μm thick. It employs the bulk silicon scientific-grade CCDs as a target for interactions of dark matter particles. The principle of detection with a CCD is illustrated in *Figure 1.5*. The charge produced due to the interaction between the ionizing particle and the silicon bulk, drifts towards the pixel gates, where it is store in potential wells until the readout. After a given exposure time, the readout process starts and the charge is transferred vertically from pixel to pixel along each column until it reaches the last row, the so-called serial register. The signal is based essentially on i) ionization signals produced by the interaction of Standard Model particles with the silicon bulk of the CCDs, ii) the intrinsic detector noise composed of the dark current (explained below) and electronic noise (during readout time) and iii) (if we are lucky) the dark matter signals, through absorption or nuclear/electronic recoil [32]. In other words, these signals from ionizing particles, known as tracks, are energy deposited in silicon pixels along the particle trajectory within the silicon bulk of the CCD.

Dark current consists of the charges generated in the detector when no outside radiation is entering the detector (spontaneous creation of electron holes due to thermal energy, defects on the crystalline structure of the silicon, etc). DAMIC CCDs have the lowest dark current ever measured in a silicon detector: 4 $e^-/mm^2/day$, limiting dark matter detection over 1.2-30 eV (limit that would put a constrain in the search of hidden photons) [42] [43].

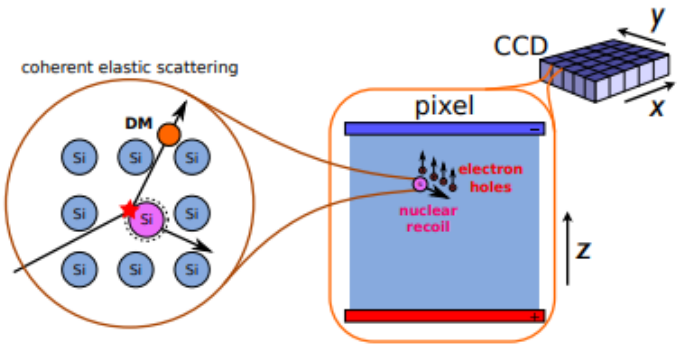

Figure 1.5: Dark Matter detection principle via nuclear recoil inside the CCD. The scattering of a DM particle with a Si nucleus leads to ionization inside the CCD bulk. Then, the charge carriers are drifted along the z axis to the CCD surface. [23]

The CCDs are made of n-type high resistivity silicon wafers that become fully depleted (active over the whole volume) at a $\leqslant$ 40 V potential applied to a thin back-side contact. Each CCD is epoxied to a silicon backing (known as dead layer as it has no detection power) together with a flex cable, used to apply the needed voltage required for the measurements. All these components are supported by a copper frame to complete each CCD module, which are inserted into a copper box cooled at 130 K inside a vacuum chamber. This copper box is later shielded against environmental radiation with lead (heavy nuclei that protect against charged particles) and polyethylene (that due to its high hydrogen concentration protects against neutrons). The setup used for the SNOLAB

experiment can be seen in *Figure 1.6*.

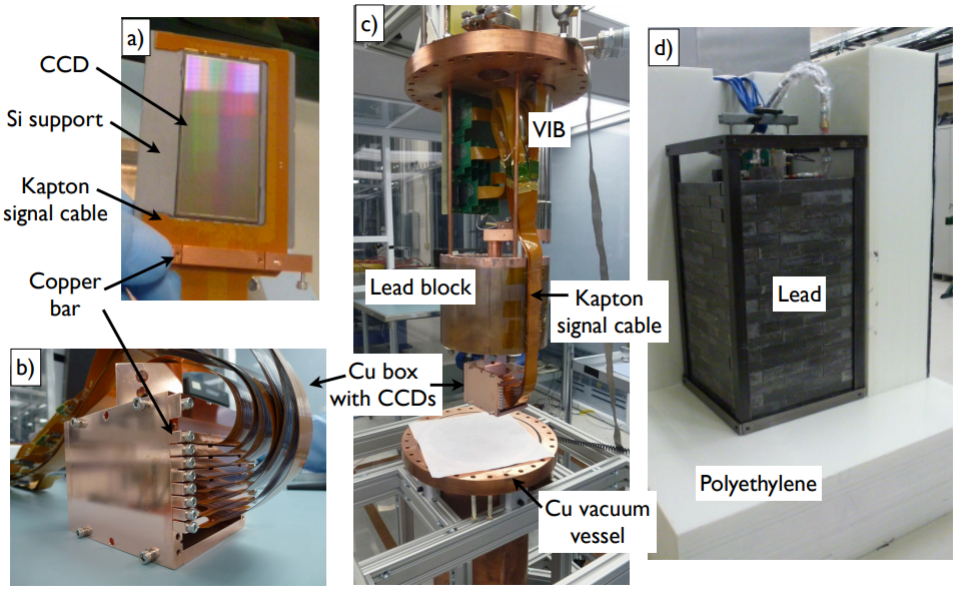

Figure 1.6: DAMIC experiment in SNOLAB [44] a) A packaged DAMIC CCD. b) The copper box housing the CCDs. c) Components of the DAMIC setup, ready to be inserted in the vacuum vessel. d) The vessel inside the lead castle, during the installation of the polyethylene shield.

DAMIC-M Experiment

DAMIC-M (which stands for DAMIC at Modane) is the next generation of the DAMIC detector, has received an international recognition, being supported by an European Research Council (ERC-Advanced grant) and also a National Science Foundation.

DAMIC-M, with the most massive ever built CCDs (1-kg detector made of 50 skipper CCDs with 36 Megapixels over a 9cm $\times$ 9cm area) will be installed at the *Laboratoire Souterrain de Modane* in France (in 3-years from now), located 1700 meters below Fréjus peak. These are the most massive ever built CCDs, with an improvement made by the Lawrence Berkeley National Laboratory: the "'skipper" amplifier [45]. The skipper amplifiers measure the charge collected by each CCD pixel several uncorrelated times, decreasing the pixel noise by averaging over a large number of samples. The readout noise achieved with 4000 samples is 0.068 electrons (0.26 eV) [46]. This makes the readout noise negligible and therefore makes dark current the limiting noise.

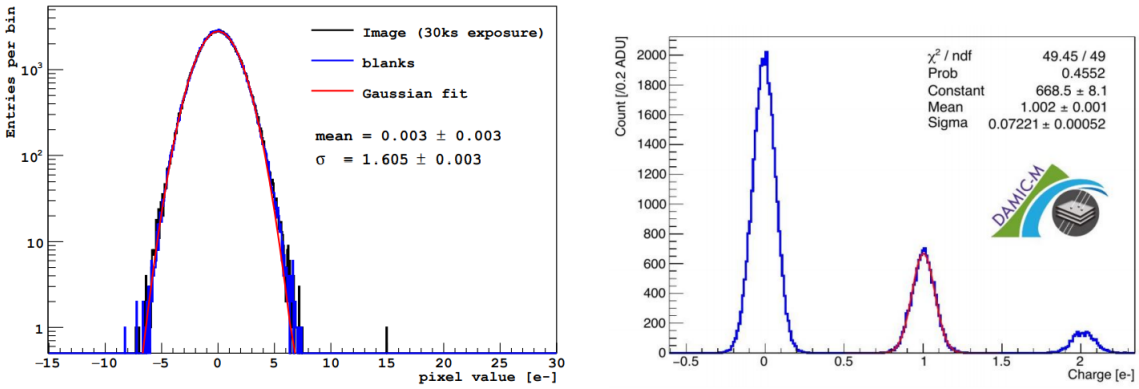

Figure 1.7: Left: Readout from DAMIC CCDs without the skipper amplifier. The readout noise is $\sigma \approx 1.6\ e^-$, making a continuous distribution due to the error greater than an electron. [32] Right: Readout performed by DAMIC-M collaboration using a prototype skipper CCD. The readout noise is $\sigma \approx 0.07\ e^-$ making the distribution strictly discrete as the low readout noise allows to distinguish perfectly between signals from one electron, and no signal. This makes readout noise negligible. [44]

When compared to other DM detector types, CCDs present some unique properties, that allows to reach very low masses, particularly in model which implies electron scattering where CCD DM detectors expect to have sensitivities similar to accelerator searches (see *Figure 1.4*). The crucial innovations in the DAMIC-M CCD detector are:

1. Unprecedented single-electron resolution by including *skipper readout*: 0.1 e^- for $<$ 1rms pixel readout time. R&D lead by Fermilab within the SENSEI group is already underway and Javier Tiffenberg have receibed a price for this achievement. See *Figure 1.7*.

2. Extremely low leakage current (intrinsic detector noise) will be achieved by including IR shields (layers of polyethylene and Lead surrounding the detector) and by operating the skipper CCDs at temperatures close to freeze-out.

3. Exquisite spatial resolution and 3D reconstruction, simulations show the ability to eliminate backgrounds (such as the intrinsic ^{32}Si) by rejecting pairs of events consisting with the same origin. See **Section 2.2.1**: the *Diffusion* model to better understand this intrinsic feature of the CCDs.

Low-Background Chamber: the proof-of-concept of the DAMIC-M detector

However, in this work, the simulations were done using the Low Background Chamber (LBC from now on) which is an experiment at Modane, starting end of this year or early next year, to test the CCD readout and other features for DAMIC-M (data taken, electronics, etc) with 2 CCDs like the ones that will be used for DAMIC-M. Other important goal for LBC is to test the background models and do some science.

As the Low background chamber design is almost finished (the chamber will start working next year), this work will be concentrated in the study of the background noise and particle signatures in this prototype. Once the DAMIC-M design is done completely, this work could be extended to the full experiment.

LBC experimental setup will be explained in **Section 2.1.1** by using the geometry for the simulations.

Backgrounds study

A challenge to the detection process is the background noise, leaving signals which could obscure the DM detection. Some of the main background sources are:

- the environmental radioactivity including airborne radon and its daughters.
- radio-impurities in the detector construction and shield material.
- neutrons from (α, n) and fission reactions.
- cosmic rays and their secondaries.
- activation of detector materials during exposure at the Earth's surface.

A careful study of the radioactive background in order to decrease it below 0.1 keV/kg/day is needed for the Dark Matter direct detection. This is done through improvements in the experiment design, the selection of the construction materials and through radioisotopes simulations for the background study.

Environmental radioactivity is controlled in the facility with a good ventilation system to avoid radon, along with the shielding for the CCDs (explained better at **Section 2.1.1**).

Usually in Copper or Lead ores from mines there are contaminants present such as Uranium or part of its decay chain. This leads to noise created by radionucleides, i.e. radioactive contaminants in the materials that conform the experimental setup. One of the main contaminants to be found is ^{210}Pb because of its long decay lifetime ($\approx$ 22 years). Whenever one of this radioisotopes decay, they leave a trace in form of a beta particle (electron or positron) or in the form of an alpha particle, followed by gammas from the de-excitation of the consequent new atom. That's why alpha particles and electrons were chosen for the simulations in this work.

It can also happen that highly energetic particles such as muons from cosmic rays excite certain nuclei, leaving it in an unstable state and thus radioactive. This is called "activation". The activation process that matters the most for this experiment is the activation of silicon by muons, leaving ^{3}H and ^{3}He nuclei. Because of muons being Minimum Ionizing Particles (MIPs) they travel further than other particles crossing matter, and therefore are more likely to reach the detector (although the number of muons received should be low, that's why the experiment is carried underground), and that's why they were chosen for the simulations too.

1.4 Aim of this study

This work was initiated by the need for an accurate validation of the DAMIC-M simulation software: DAMICG4 and psimulCCDimg. Two main particles have been used to achieve that: simulation of muon particles are used to validate the Diffusion model (how the electron-hole pairs drift towards the pixel gate, see **Section 2.2.1**), while alpha particles for the CCD Saturation (see **Section 2.2.1**), as well as, the energy dependence on the diffusion model. As DAMIC-M and LBC are not yet running, we used the diffusion model parameterized for data taking with the DAMIC experiment.

DAMICG4 simulates particles crossing through the detector materials, along with their decays and interactions, using Geant4 (a simulation software that uses Monte Carlo methods to study the passage of particles through matter, see **Section 2.1**: Geant4 Overview, for more information). On the other hand, psimulCCDimg reconstructs the CCD behaviour, introducing processes not simulated by Geant4 like the electron-hole pair creation within the silicon bulk, how this pairs are drifted towards the readout electronics, the readout noise, the dark current or the pixelization along the CCD by using Python scripts. A better explanation will be given in Chapter *2*: Methodology.

Both software (first DAMICG4 to see how particles reach the CCD and then psimulCCDimg to emulate the CCD behaviour) are used together to analyse background noise. This includes radioisotopes, taking into account the already measured radiopurity of the materials, cosmic ray particles, noise from the electronics, etc.

Once analysed and fully understood, the background noise is then compared to the real experimental data when DAMIC-M experimental measurements end.

From this study, the simulations have been used for the creation of a solid database as inputs for a machine learning algorithm design with the goal to be able to distinguish between different particle tracks within the CCD image results automatically.

2 — Methodology

The first main goal of this work was the validation of the software that will be used to model the background of the DAMIC-M detector. An intrinsic background of less than 1 e-/kg/day/keV is required to fully exploit DAMIC-M scientific reach on the hidden sector. Despite most of the DAMIC-M components have optimal technical solutions to achieve such background level from the original DAMIC, some other components (the larger size of the CCDs requires a new device package and box, kapton cables, infrared shielding layers, ...) need to be re-designed and tested from scratch. This include a complete simulation-based data analysis to assure each change on the design still guarantee the desired background level. These studies of background mitigation are currently under way and use this software. It is therefore crucial to ensure that the software works properly under any type of particle of the standard model. In particular, I validate the functionality of the software when simulating muons and alpha particles passing through the LBC geometry, understanding deeply their signatures at the CCDs. This can be use to provide enough simulated CCD images to be used in machine learning algorithms (mostly focused on pattern signal recognition of standard model particles, as well as, to identify malfunctionalities of the detector).

The software used to mimic the response of the DAMIC-M CCDs is composed by two packages: **DAMICG4** and **psimulCCDimg**

- **DAMICG4** performs Geant4-based simulations of the detector; being Geant4 a C++ framework which relies on Monte Carlo (MC) modelling to emulate physical processes [47];
- **psimulCCDimg** is a Python3 module used to reconstruct the response of the detector [48].

Roughly speaking, each background source is simulated with DAMIG4 (presented from some general remarks about the simulation package Geant4 in **Section 2.1** to the detector geometry used for this study, i.e. the Low-Background Chamber (LBC) in **Section 2.1.1**). The software simulates the passing of particles through the detector by simulating its interaction with the different materials [1]. The output of the simulation is a collection of geometrical points inside the detector (i.e. the CCDs) where the particles have lost energy. This collection of energy losses feeds **psimulCCDimg** used to mimic the CCD's response (depicted in **Section 2.2**): convert the energy losses to electron-hole pairs, drift and diffuse those charge carriers to the collecting electrodes, pixelize the signal, and simulate the intrinsic detector noise. To finally clusterize the signal, i.e. find the signature of each particle in the CCD image (see *Figure 2.7*). The output file format is ROOT, a framework for data processing developed by CERN written in C++. ROOT tools were mainly designed for particle physics data analysis, but it is a framework used in many other fields [49]. In the following sections more details of these processes are given.

[1] This primary particles could create secondaries due to its interaction with the matter and they are also tracked.

2.1 Geant4 overview

Geant4 is a free software and the last in the Geant series of software, designed to simulate the passage of particles through matter using Monte Carlo methods. Geant name is an acronym for GEometry ANd Tracking, as it allows to the creation of a geometric space with materials to be simulated, and tracks the particles involved. It was originally developed at CERN in the 1970's and written in FORTRAN [50], but as time passed and the code grew in complexity, the need for object orientated techniques appeared and in 1998 the first version of Geant4 was created written in C++ [47]. Geant4 development, maintenance and user support are taken care by the international Geant4 Collaboration [51].

A Geant4 simulation can be thought of as proceeding through a series of steps:

- **Primary Particle**: the particles to be simulated (launched) are specified, choosing which particles are, if they are to be excited or on ground state, initial kinetic energy, direction, position, etc.
- **Physics Lists**: the process a particle is allowed to undergo, and the model describing each process is chosen (several models are available for each energy range);
- **Geometry:** the geometry of the system is defined, as well as, the materials of each component of the system. Two key elements on every geometry definition in Geant4 are set by default: the "World" volume and its internal reference frame. The "World" volume is conceived as all the three-dimensional space considered by the simulation (as if it was a perfect vacuum), while the internal reference frame is a Cartesian system with the "World" center as its origin. The rest of the system in any geometry is defined by creating a geometrical volume for each component, which center rests at some point in the internal reference frame of another volume (usually in the internal reference frame of the "World" volume). An example with just the "World" volume, the reference frame axis and the sensitive detector volume is shown in *Figure 2.1*.
- **Sensitive detector:** each component of the geometry that is a sensitive sensor must be marked as so. A sensitive detector is the part of the geometry from which the output is taken (not every particle trace is recorded, just the needed ones, in order to be compared with data taken). In this particular case, the sensitive detector is the active region of the CCDs.
- **Run:** When all this "predefining" is done, the run itself starts, generating primary events (the primary particles start moving in the geometry in a discrete movements, i.e. step by step).
- **Tracking:** As the primary particles are transported through the system in little steps, in each point, they interact with the materials (in the provided processes). Each interaction with an energy loss is considered a **Hit**. Hits might produce secondary particles, which are simulated too (secondaries might create another set of secondaries until the 'last' secondary particle has lower energy than a given threshold).
- **Energy cuts:** The energy threshold and step size are tuned parameters used for computational time optimization while reproducing the real process as much as possible, so particle in

each material should have its own energy threshold. This parameters are optimized individually for each experiment.

- **Output:** The energy losses and particle productions inside the sensitive detector are stored to simulate the response of the detector with psimulCCDimg.

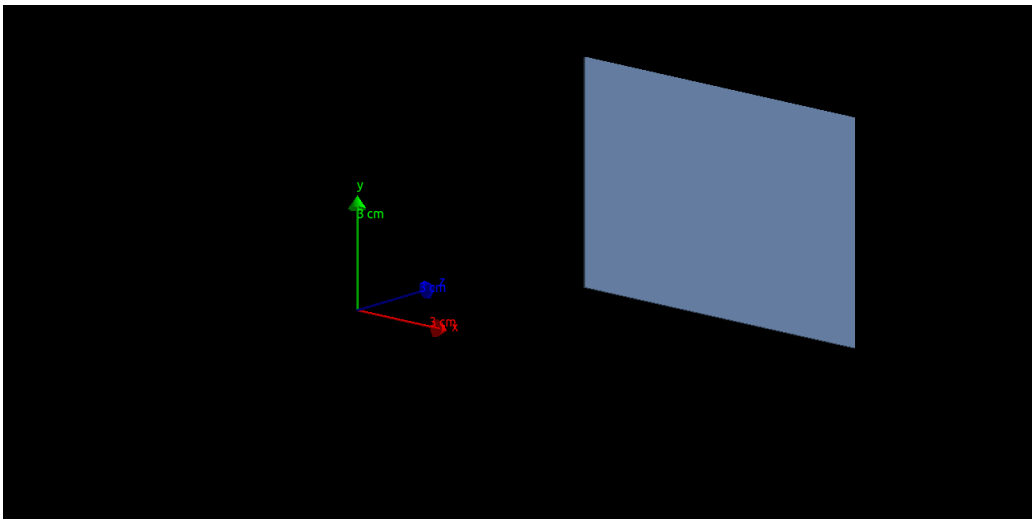

Figure 2.1: Geant4 LBC geometry with just the "World", the reference frame axes and the sensitive detector (CCD).

The simulation process can be understood better with an example. An electron is simulated outside the CCD in a geometry in which there is only a monomaterial CCD and the "World" ("World" is the Geant4 geometry containing the full detector you want to simulate, i.e. used to define the end of your geometry). *Figure 2.2* shows an sketch of the tracked electron, step by step within the CCD (for this simplistic example). In each of the steps, all physical process defined for your physics lists are invoked and the most probable is applied: energy and momentum are computed to define the next step. Now the particle moves to the next step, if this belongs to the same material, if not, the step length will be shorter and the particle moves to the border between the two materials and/or volumes. This procedure is done until the particle is killed: it arrives to the World, or its energy is lower than a given threshold, or is killed by another process.

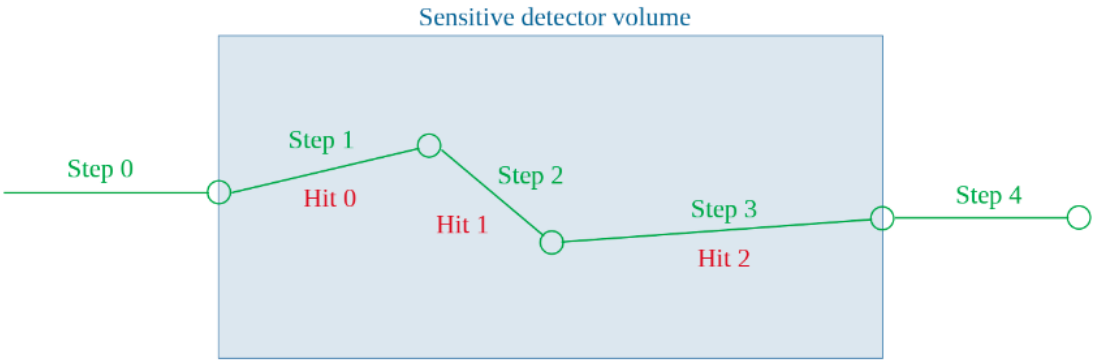

Figure 2.2: Geant4 simulation scheme. It shows the step and hit process typical from the Geant4 algorithm.

2.1.1 LBC Geant4 geometry

The Low Background Chamber (LBC) is an experiment set up in Modane in order to test the new CCDs for DAMIC-M. It works as a "small" prototype, in the sense it has 2 CCDs instead of 50 (like DAMIC-M), but the external experimental setup will be similar in both cases, and this work can be extended to DAMIC-M.

The LBC geometry consists in:

- A sensitive detector: two 4000x6000 pixels (15x15 μm, 675 μm thick) CCDs composed of silicon and polysilicon layers.
- Kapton cables, for the electronic imput.
- A copper frame for the CCDs.
- Roman lead (taken from a spanish galleon) for protecting the CCDs from ionizing radiation while not radiating itself (because of being old, the decay time for lead nuclear chain has already passed and thus it does not induce more background noise).
- "New" lead extra layer (new lead is cheaper than the old one and radiopurity this far from the sensitive detector is unnecessary).
- External cryostat to maintain the temperature at around 130 K.

The final experiment also has a polyethylene external layer in order to provide a shielding against neutrons from cosmic rays and nuclear decays, preventing nuclear activation. The shielding works due to the high content of hydrogen atoms in polyethylene. It is not necessary for the purposes of this simulation, as it should have negligible stopping power on muons or electrons, and therefore it is not included in the LBC geometry.

All these layers are shown from inside to outside in *Figure 2.3*.

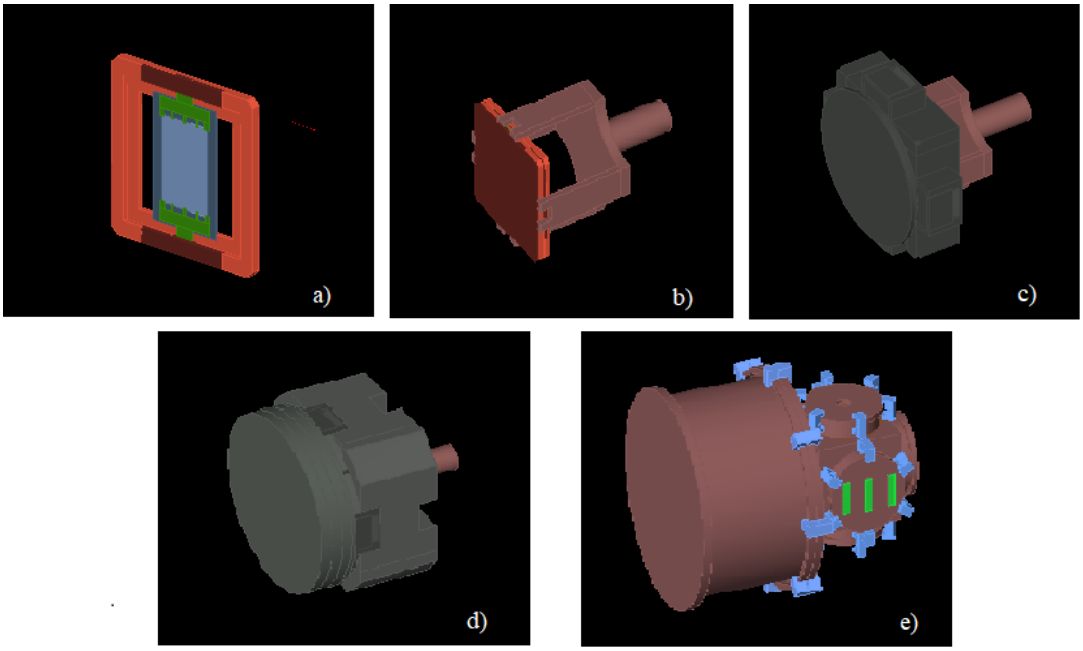

Figure 2.3: a) CCD module including the sensitive detector zone (light blue), kapton cable (green) and copper frame (orange). b) Copper box holding both CCD modules. c) Roman lead layer. d) "New" lead layer covering the Roman one. e) Whole LBC geometry including cryostat layer. In light blue are represented holder pieces and in green the electronic input for the cryostat.

2.1.2 Running DAMICG4

First of all, the initial state of the simulation must be defined, i.e. the 'primary particles'. Once this is done, Geant4 will track the particles through the system until they stop, decay or are transported beyond the limits of the "World" volume.

The generation of the primary events in the present application was done by creating a Python script (shown in Chapter *5*) that generates Geant4 macro files. These macro files are executed by DAMICG4 using the particle gun internal class from Geant4, which creates a beam of particles by defining their type, position, direction of motion and kinetic energy.

The chosen particles for this work are muons, alphas and electrons. Highly energetic muons come form cosmic rays being minimum ionizing particles (MIPs) and therefore crossing through almost every material loosing little energy. Because of it, they can reach the detector and leave traces in it. They can also activate some nuclei producing radioisotopes. Alphas and electrons both come from radioisotopes, either alpha or beta decay respectively. All these are the expected particles, along with gammas, but gammas are discrete process, being its secondary the tracked one.

MIPs are launched isotropically from the copper frame holding the CCD in order to emulate the particle shower from cosmic rays. On the other hand alpha particles (as they travel very short

distances) are generated inside the sensitive detector, in case there are impurities in the CCD materials. Isotopes are always generated in their original materials (for example ^{210}Pb is generated in the copper frame, and in any other layers that could have lead impurities), and are given null initial kinetic energy, because they are expected to decay from an still state.

2.1.3 Example simulating a ^{60}Co radioisotope

As an example of a Geant4 run, a Cobalt-60 isotope is simulated. Cobalt-60 is taken as an example because its only possible decay mode is a beta decay (emission of an electron and a neutrino) followed by a de-excitation of the Nickel nucleus (gamma emission) (see *Figure 2.4* for the decay scheme of ^{60}Co), making the output easier to follow. This allows a better understanding on how DAMICG4 works.

One ^{60}Co isotope is generated in a random position inside the sensitive detector (CCD) volume of the LBC geometry with no initial kinetic energy. The run is started using the macro file shown in Appendix I (Chapter *5*).

The output obtained from Geant4 contains a long list (almost 12000 lines for this little example) of the tracked particles as shown in *Figure 2.5*. It is a great source of information because it contains the position of the particles and their kinetic energy, along with the processes taken into account and the volume traversed at every step. The ^{60}Ni nucleus in an excited state decays emitting a gamma, which is transported through the volumes and suffers Compton scattering (comp), Rayleigh scattering (Rayl) or photoelectric effect (phot), leaving electrons some energy lost later in ionization (eIoni) or scintillation.

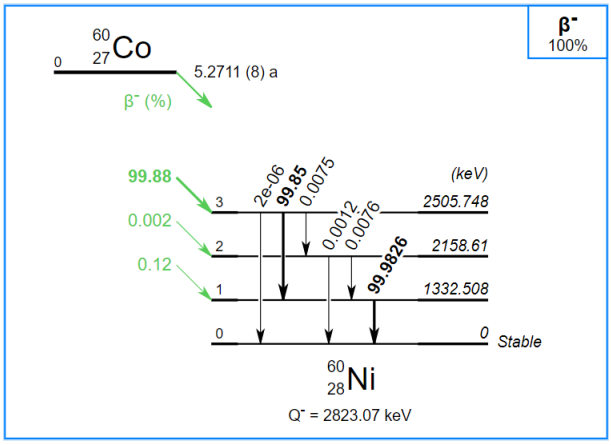

Figure 2.4: Scheme for the ^{60}Co decay.

```
*********************************************************************************************************
* G4Track Information:   Particle = Ni60[2505.753],   Track ID = 2,   Parent ID = 1
*********************************************************************************************************

Step#    X(mm)    Y(mm)    Z(mm) KinE(MeV)  dE(MeV) StepLeng TrackLeng  NextVolume ProcName
    0     22.3     26.3      150  1.24e-06        0        0         0 CCDSensor_PV initStep
    1     22.3     26.3      150         0 1.24e-06 4.25e-308 4.25e-308 CCDSensor_PV RadioactiveDecay
Track (trackID 2, parentID 1) is processed with stopping code 2

*********************************************************************************************************
* G4Track Information:   Particle = gamma,   Track ID = 908,   Parent ID = 2
*********************************************************************************************************

Step#    X(mm)    Y(mm)    Z(mm) KinE(MeV)  dE(MeV) StepLeng TrackLeng  NextVolume ProcName
    0     22.3     26.3      150      1.17        0        0         0 CCDSensor_PV initStep
    1     22.4     26.2      150      1.17        0    0.261     0.261 CCDModule_PV Transportation
    2     28.3     21.2      155      1.17        0     8.85      9.11 ColdCopper_3_PV Transportation
    3     30.4     19.4      156      1.17        0     3.19      12.3 AncientLead_1_PV Transportation
    4     33.5     16.7      159     0.869 0.000435      4.8      17.1 AncientLead_1_PV compt
    5     46.4     5.07      158     0.618  0.00305     17.4      34.5 AncientLead_1_PV compt
    6       49     5.17      156     0.618        0     2.88      37.4 ColdCopper_3_PV Transportation
    7     52.1      5.3      155     0.618        0     3.46      40.8 CCDModule_PV Transportation
    8     61.9     5.69      150     0.618        0     11.1      51.9 ColdCopper_1_PV Transportation
    9     70.5     6.03      145     0.618        0     9.68      61.6 ColdCopper_3_PV Transportation
   10     73.6     6.16      144     0.618        0     3.46      65.1 CCDModule_PV Transportation
   11     74.1     6.18      143     0.618        0    0.618      65.7 ColdCopper_2_PV Transportation
   12     77.6     6.32      141     0.213 0.000121     3.97      69.6 ColdCopper_2_PV compt
   13     76.8     4.43      144     0.213        0     2.94      72.6 ColdCopper_3_PV Transportation
   14     76.2        3      145     0.213        0     2.22      74.8 ColdCopper_1_PV Transportation
   15     74.1    -1.83      151     0.213        0     7.53      82.3 CCDModule_PV Transportation
   16     72.5    -5.54      155     0.213        0     5.79      88.1 ColdCopper_3_PV Transportation
   17     71.9    -6.97      156     0.213        0     2.22      90.3 AncientLead_1_PV Transportation
   18     70.9     -9.3      159     0.115  2.6e-05     3.64        94 AncientLead_1_PV compt
   19     70.9    -9.29      159     0.115        0   0.0243        94 AncientLead_1_PV Rayl
   20     71.1    -9.06      159         0  0.00508    0.423      94.4 AncientLead_1_PV phot
Track (trackID 908, parentID 2) is processed with stopping code 2

*********************************************************************************************************
* G4Track Information:   Particle = e-,   Track ID = 915,   Parent ID = 908
*********************************************************************************************************

Step#    X(mm)    Y(mm)    Z(mm) KinE(MeV)  dE(MeV) StepLeng TrackLeng  NextVolume ProcName
    0     71.1    -9.06      159   0.00796        0        0         0 AncientLead_1_PV initStep
    1     71.1    -9.06      159         0  0.00796 0.000453  0.000453 AncientLead_1_PV eIoni
    2     71.1    -9.06      159         0        0        0  0.000453 AncientLead_1_PV Scintillation
Track (trackID 915, parentID 908) is processed with stopping code 2
```

Figure 2.5: Geant4 output log for tracking particles from a ^{60}Co decay.

All the information from the processes occurring at the sensitive detector volume (CCDSensor_PV) is later stored as a ROOT file for analysis purposes, and is used in psimulCCDimg to simulate the CCD behaviour. The rest of the particle tracking can be useful in few cases in which the particle directionality or the information about the volumes traversed by the particle are important. But main information needed is the energy losses in the CCD the same one that data provides.

2.2 Mimicking the CCD response with psimulCCDimg

psimulCCDimg is a Python3 script made to apply a chain of processes (detector response and/or reconstruction) over Geant4 simulations, to obtain an emulation of the CCDs behaviour. This is done by applying to the obtained data from Geant4 several processes for the detector response: diffusion, pixelization, electronic noise, Dark Current and saturation. Another two processes are taken into account for signal reconstruction purposes: signal pattern recognition and cluster finding. All these processes will be explained in this section.

2.2.1 Detector response

The detector response is emulated with a diffusion process, the creation of the intrinsic detector noise, and the pixelization of the CCD module. Along with the pixelization is included a saturation value for every pixel.

Electron-hole diffusion

The diffusion process describes the transverse diffusion of charge deposition in the CCD. It can be described by a Gaussian with $\sigma_{xy} = \sqrt{2D_p t}$ where D_p is the diffusion coefficient of the holes in the silicon and t is time (assigning $t = 0$ to the moment of charge deposition) [52] [53] [54]. By using the linear relationship between drift velocity and electric field ($v_d = \mu_p E$, where μ_p is the hole mobility in silicon), the electric field profile in the CCD ($E(z)$) and the Einstein relation ($\frac{D_p}{\mu_p} = \frac{kT}{e}$ with k the Boltzmann constant, T temperature and e for electron charge) it can be obtained:

$$\sigma_{xy}^2(z) = -A \ln(1 - bz)$$

Where:

$$A = \frac{2\epsilon_{Si} kT}{\rho_n q} \;\; ; \quad b = \left(\frac{\epsilon_{Si} V_b}{\rho_n z_D} + \frac{z_D}{2} \right)^{-1}$$

ϵ_{Si} is the silicon permitivity, ρ_n the donor charge density, V_b the bias voltage across the CCD, and z_D the thickness of the active region (669 μm). From the theoretical equations and the data taken at DAMIC SNOLAB experiment the best fitting parameters for A and b were found and applied in psimulCCDimg (216.2 μm^2 and $8.86 \cdot 10^{-4}$ μm^{-1} respectively). This way, the diffusion process takes account of how the holes (which are the readout source) inside the silicon repel one another so larger energy deposits (leaving more holes) or deeper signals (more time to repel) leave larger and more diffuse signatures. Diffusion process is represented in *Figure 2.6* diagram.

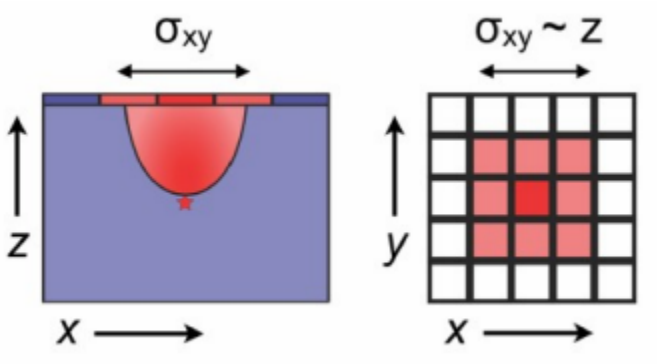

Figure 2.6: Diagram illustrating the diffusion of charge carriers as a function of depth resulting in diffused particle tracks. [23]

Pixelization

Pixelization transforms the sensitive detector volume, simulated in Geant4 as a whole, into proper sized CCD pixels. In the case of the LBC geometry, the CCDs are 4000 pixels long in the x axis and 6000 in the y axis, with $15x15$ μm size each pixel.

Intrinsic detector noise

The electronic noise accounts for the skipper amplifier readout noise. Although it is a negligible source of noise, every known source needs to be simulated. The values given to psimulCCDimg are the ones explained in **Section 1.3**.

Dark current is the main internal source of noise (excluding external background from radioisotopes, etc) thanks to the skipper amplifiers. It is related to the spontaneous creation of electron-hole pairs in the silicon due to crystallographic defects and thermal excitations, and has a Poissonian profile (with exposition time).

Pixel Saturation

The saturation process limits the energy deposits per event and pixel, as a pixel can only read a certain amount of holes in a given time. The saturation limit in the CCDs is around 17 keV so pixels are only saturated by large energy deposits such as alpha particles, or several particles at the same time (not expected).

2.2.2 Signal reconstruction

For reconstruction two processes are used, signal pattern recognition, which allows to distinguish the noise or dark current signals from the particles (putting a threshold on pixels, as pixels charged with one or more electron have a signal different from noise), and the clusters recognition process,

that distinguishes between different clusters (group of pixels with signal that are adjacent one another, normally different particles belong to different clusters) depending on how far is a charged pixel from another (usually two pixels is the furthest diffusion can drive two holes from the same particle interaction).

All these processes combined can be better understood using an image from the debug mode of psimulCCDimg like the one shown in *Figure 2.7*.

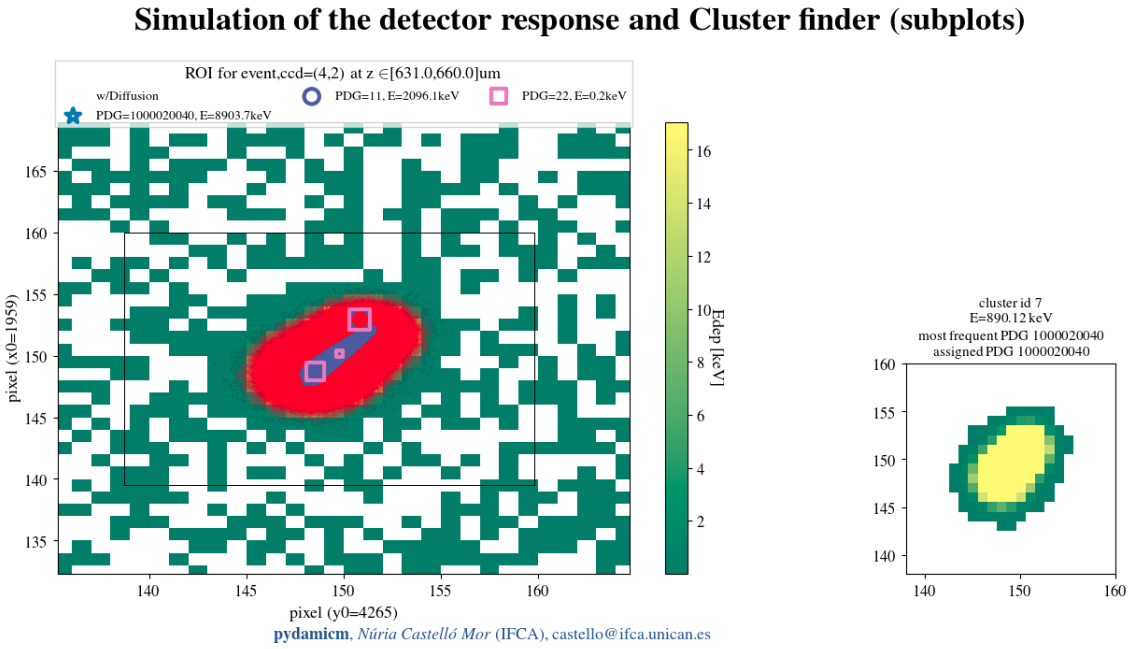

Figure 2.7: Debug mode picture from a low energy alpha particle sample. It can be seen in the left picture how the intrinsic noise is emulated through all the CCD with the green pixels. Red dots are electron-hole pairs driven by the diffusion process, while the pink squares are Hits from DAMICG4. Thanks to the signal reconstruction processes, at the right picture is shown the alpha cluster, equivalent to the cluster in the middle of the left image (in blue).

These processes altogether allow the emulation of the DAMIC-M CCDs behaviour, and with it, the reconstruction of the background noise spectrum, being able to compare it with the experimental data when the real experiment is done, and finding strange signals that can be dark matter candidates.

3 — Results and analysis

In this chapter, the simulation relevant results will be presented for both muons in **Section 3.1** and alpha particles in **Section 3.2**, along with their analysis for either the software validation and the database creation for the machine learning algorithm.

Muons and alphas have been simulated and analysed in order to understand the CCD response to different energy deposits, thus being able to validate both DAMIC-M software and to create the database. As already mentioned, the muons are used to validate mostly the Diffusion model. As particle alphas loss a huge amount of energy in a single point, they are used to validate the energy dependence of the diffusion model with the energy, as well as the saturation of the pixel. The expected signatures for different particles is shown in *Figure 3.1*.

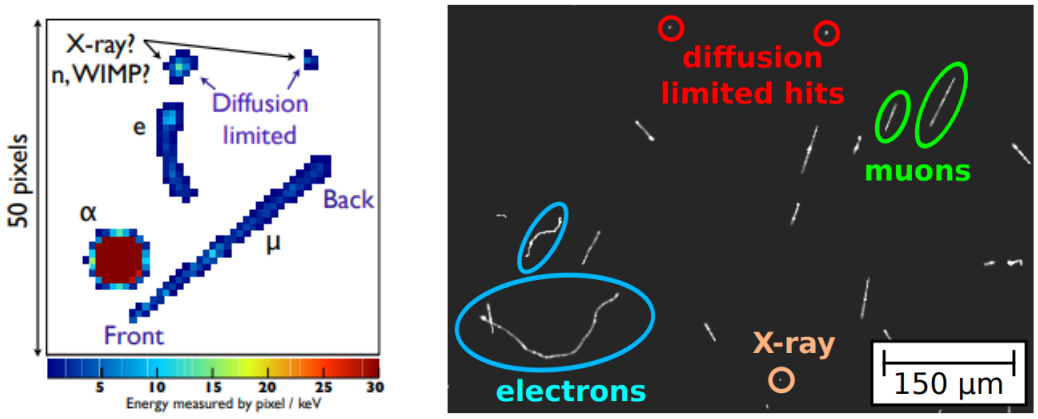

Figure 3.1: Left: 50x50 pixels segment of a DAMIC image when exposed to a ^{252}Cf source on the surface. [23] Right: Sample of tracks recorded at sea level from a DAMIC CCD. [55]

Muon tracks are elongated because they cross the whole CCD with very little interaction, while electrons are less massive and more interacting, so their signatures are bent. Alphas are big and round because they leave all their energy in a little region (driven by plasma effect [56]), saturating most of the pixels in their track. Point like sources, such as gamma particles, neutrons, or dark matter candidates themselves are called diffusion limited because their shape and size is entirely created by the diffusion process. The latter are the most interesting in direct detection of dark matter.

3.1 Muon analysis

As said in **Section 1.4**, muon simulations are necessary, not only for the creation of the database for the machine learning algorithm, but for the validation of the diffusion process. Muons are useful for this goal because of being MIPs, allowing long tracks where the diffusion can be perfectly distinguished.

120000 muons (μ^-) at different energies have been simulated from the Copper frame that holds the CCD. 10000 muons were generated at each different energy (500 keV, 2 MeV, 8 MeV, 32 MeV, 125 MeV, 500 MeV, 2 GeV, 8 GeV, 32 GeV, 125 GeV, 500 GeV and 1 TeV). The energy spacing is logarithmic in the MeV and GeV scale separately because the differences in muon traces are expected to be very low. The few changes expectancy comes from muons being a minimum interacting particle in this energy range, as can be seen in *Figure 3.2*, the muons Stopping Power profile. 150000 positive muons (2 GeV μ^+) have also been simulated to check if there is any difference between μ^- and μ^+ CCD signals. Also, we want to have a big statistic around a few GeV (2 GeV, for example) because the mean energy of muons reaching the Laboratoire Souterrain de Modane (LSM) is around $\approx 4\ GeV$. Muons below an energy of 2GeV do not have enough energy to reach our detector (remember, that the lab is underground), however we decided to simulate muons below that energy to check the code even with non expected signals.

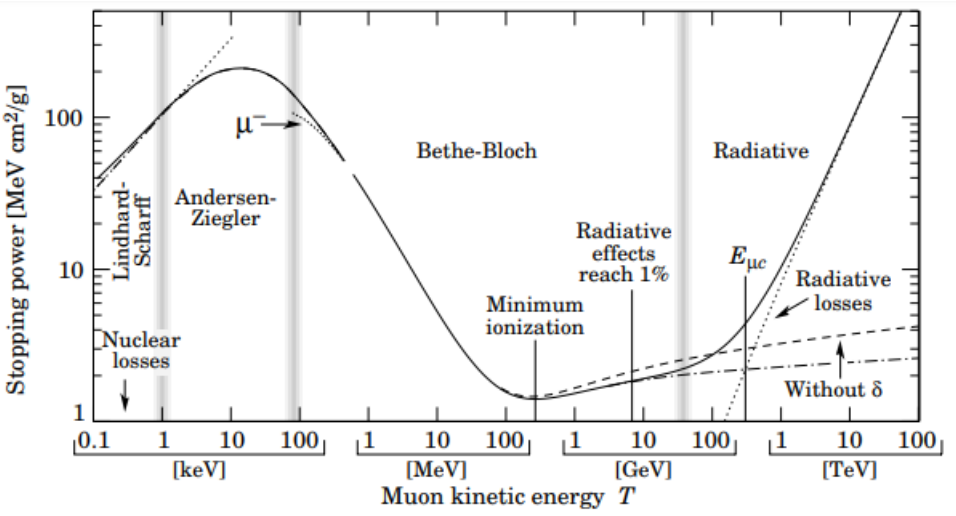

Figure 3.2: Muon Stopping power profile depending on the particle's kinetic energy. Although this profile is for muons in Copper, the profile shouldn't differ abruptly. [57]

The differences in muon traces could come at low energies (500 keV), where muons are more ionizing and are thus expected to deposit more energy into the CCD electron. Also, less muons are expected in this energy range, due to the deep depth underground the experiments are located ($\approx$ 1700 meters). By the time the muon flux arrive to the laboratory, low energy muons should have been stopped by the rock above. Expected muon are over the GeV and below the TeV regime where the radiative losses start.

Despite of muons expected experimentally as a shower from above the detector, they were simulated isotropically for a better understanding of the internal simulation and reconstruction processes. Muons information is not only valid for understanding muon behaviour, but also can be extended for any minimum ionizing particle (as it was found out later that happens to stripped protons from Silicon nuclei).

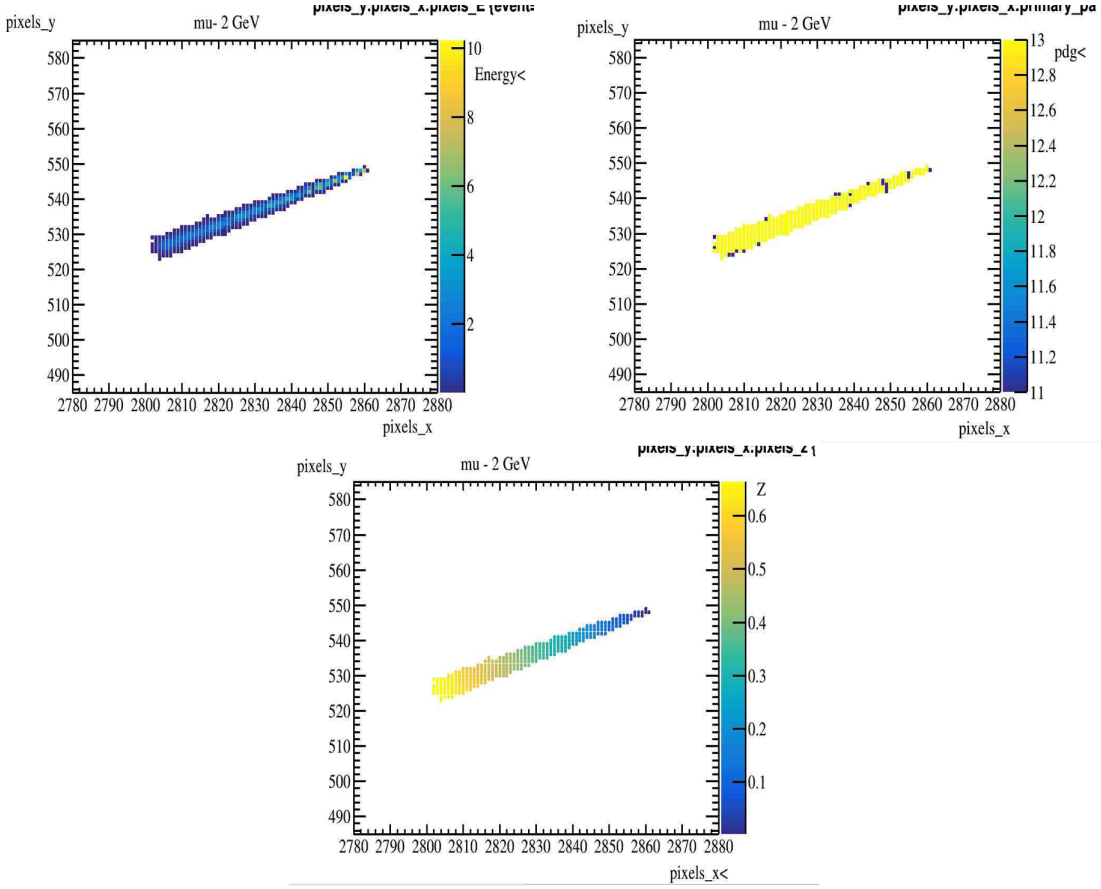

Figure 3.3: 2 GeV muon track as seen in the CCD pixel by pixel, changing the color code information. Top Left: Track showing energy deposit in each pixel (yellow for greater energies, while blue for lower ones, in keV). Top Right: Track showing which particle leaves the greatest amount of energy in each pixel (13 (yellow) for muons, 11 (blue) for electrons [58], see Monte Carlo particle numbering scheme). Bottom: Track showing the energy deposit's depth within the CCD (yellow for deeper signals, blue for closer to the readout surface ones, in mm).

Figure 3.3 shows a 2 *GeV* simulated muon track, this signature fits perfectly compared to the expected signatures from *Figure 3.1* found in data. This proofs that the simulation works fine, the energy deposits are regular and mainly left by the muon passing through, as expected from a minimum ionizing particle (else, the ionized electrons would be dominating the energy deposits). The track is baseball-bat shaped from a thinner part in the top of the CCD to a thicker part for the

deepest energy deposits as expected from the diffusion process. All this means that the simulation software works as expected and drives the particles' signature shape and size. Note that we do not have data to compare with, and the Diffusion parameters are the ones calibrated for DAMIC data, while the intrinsic noise parameters are the expected ones for DAMIC-M and the LBC experiments.

Tracks length or shape are independent on initial kinetic energy because muons cross the whole CCD, and the ionization energy losses are quite the same, as it is known from *Figure 3.2*. This is proven in *Figure 3.4* where muons with two very different energies were generated and the energy deposits in each pixel do not differ much.

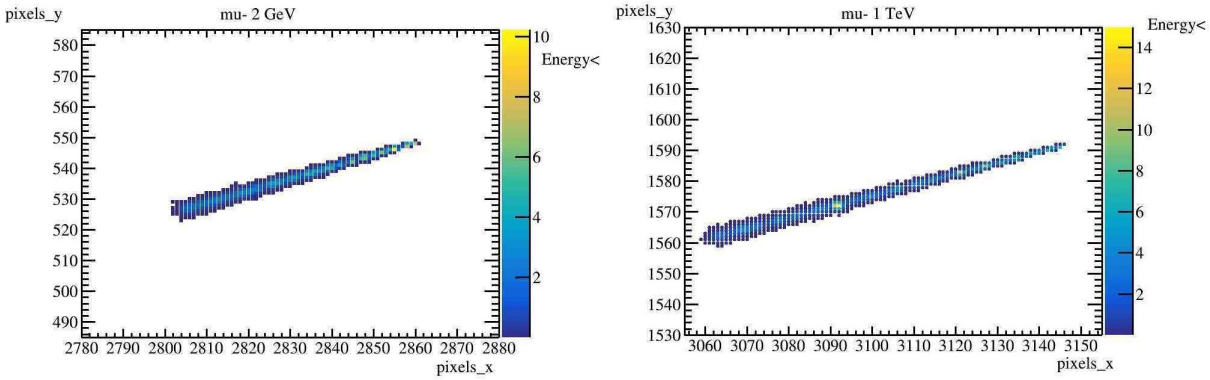

Figure 3.4: Muon tracks for different initial kinetic energies. It can be seen how typical muon tracks do not differ much one from another. This is reinforced and extended to every track in Figure 3.5.

The number of simulated muons interacting with the CCDs increase with its initial kinetic energy because muons can ionize more electrons with more energy, and the radiative losses slope starts, leaving the minimum ionization valley (*Figure 3.2*). So in the range of 2 GeV to 1 TeV, there is an increasing ratio from 0.05 to 0.1 approximately, meaning there are $\approx$ 500 clusters detected from 10000 muons simulated at 2 GeV and 1000/10000 at 1 TeV. But it is important to keep in mind that this ratio could be greater than 1, as a muon can leave more than one cluster (for example, the muon itself and an striped electron from the copper frame; or for instance, the muon can interact with the two CCDs and two different clusters will be considered, one in each CCD).

So with a low statistics but sufficiently large for the purpose of this work (between 500 and 1000 muons per energy), the muons' behaviour can be properly analyzed and understood. Despite the amount of muons expected at Modane is not significant, its interaction with the detector (the secondary particles produced due to its interaction with heavy materials) can produce clusters at lower energy where dark matter is expected. Its understanding is then really important. Note that all data simulated in this work will also be used for other purposes (like the already mentioned creation of the database for the machine learning algorithm).

Analysis of the distribution of the clusters on the XY plane of the CCD

The analysis of the homogeneity and isotropy of these particles in the CCDs have been made, along with studies on the energy deposits of muons. The homogeneity and isotropy study check that muon tracks are received in the same amount and way in every part of the CCD.

The homogeneity on the clusters distribution in the x-y plane will be done using different methods, but this is still a work in progress. The methodology used to check for homogeneity is as follows: divide the CCD in different grids (regions) and study how change the number the number of cluster in each region of the grid. This was done using the variation coefficient, the ratio of the standard deviation to the mean. This statistic is a coefficient used to express homogeneity. A consensus has not been reached around what value of the variation coefficient should be used to classified a data set as homogeneous, but the closer the parts of the grid are to the mean value between them, the more homogeneous is the cluster distribution.

Understanding the simulated muon signature

On the other hand, isotropy has been tested using track's length. If muons reach the CCD from any part of the lab, as expected, muons hitting the CCD with higher angle (incident angle with the CCD XY plane) have longer tracks than those hitting the CCD with smaller angles as the tracks are seen from the XY plane. The test is done comparing DX and DY, where DX (and analogously any axis) is the difference between the last reached pixel and the first. For example, in *Figure 3.3* the muon's signature goes from the pixel 2800 in the x axis to 2860 approximately, meaning DX=2860-2800=60 pixels. As the z-axis isn't pixelated, DZ is set in millimeters and goes from 1 to 1.67 [1].

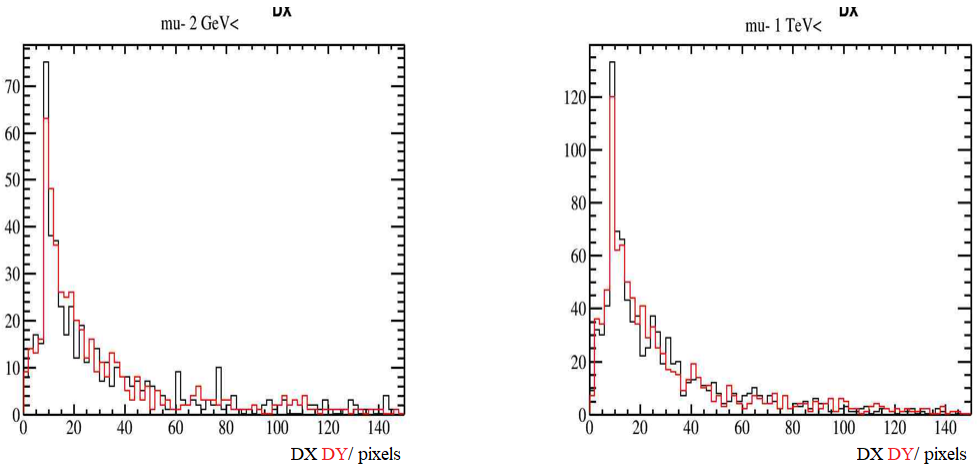

Figure 3.5: Comparison for muon tracks elongation between axes. The DX distances are shown in black while DY distances are shown in red. Units on the X axis are pixels.

[1] it starts in 1 because otherwise there could be a 0 in the z-axis while x and y pixels starts in 1 and this was problematic for coding

The distribution of the cluster elongation (see figure *Figure 3.5*) peaks at around ≈ 10 in both axis (DX and DY), which means that those muons hitting the CCDs with a certain angle will be more probable than the others. Indeed, there are many more muons with shorter signatures than longer ones, reflecting the CCD geometry: the CCD's depth (z-axis) is way shorter than the length or width (60x90x0.67 millimeters).

It is worth noting that we may have a biased simulation due to the fact muons were not simulated coming from the walls, instead they were placed randomly in a closer volume (copper frame and copper plate on top of the CCD acting as a cover) to the CCDs mostly to computational reasons. The muons placed on the cover on top of the CCD could forbid some bigger angles and therefore some longer muon tracks, but this result is still expected in the real experiment, mainly because of the CCD geometry and the cosmic flux expected at Modane. All that make the perpendicular-to-the-CCD muon angle the most probable angle (if they come perpendicular to the CCD, which surface is pointing towards the sky, muons travel through less ground and reach the laboratory more easily than others with greater angles).

Cluster Energy distribution

The energy of the cluster are shown in *Figure 3.6*, finding the same profile for every initial kinetic energy (omitting tiny statistical deviations). There are two strong peaks, one related to 0 keV, meaning a great amount of particles with very low energy arriving at the CCD, and the other around $\approx$ 250 keV. The initial hypothesis is that the peak around 250 keV is related to muons crossing the CCD perpendicular to the x-y plane (the most probable ones, as it is shown in the previous test). A quick calculation from stopping power multiplied by silicon density and distance traversed if muons are perpendicular:

$$1.6MeV\frac{cm^2}{g} \cdot 2.33\frac{g}{cm^3} \cdot 0.067cm \approx 250keV$$

While the 0 keV peak is not related to muons, but to other particles, mainly stripped electrons from copper, arriving at the CCD with very low energies, as well as pixel charged due intrinsic noise that was not properly filtered by the reconstruction process.

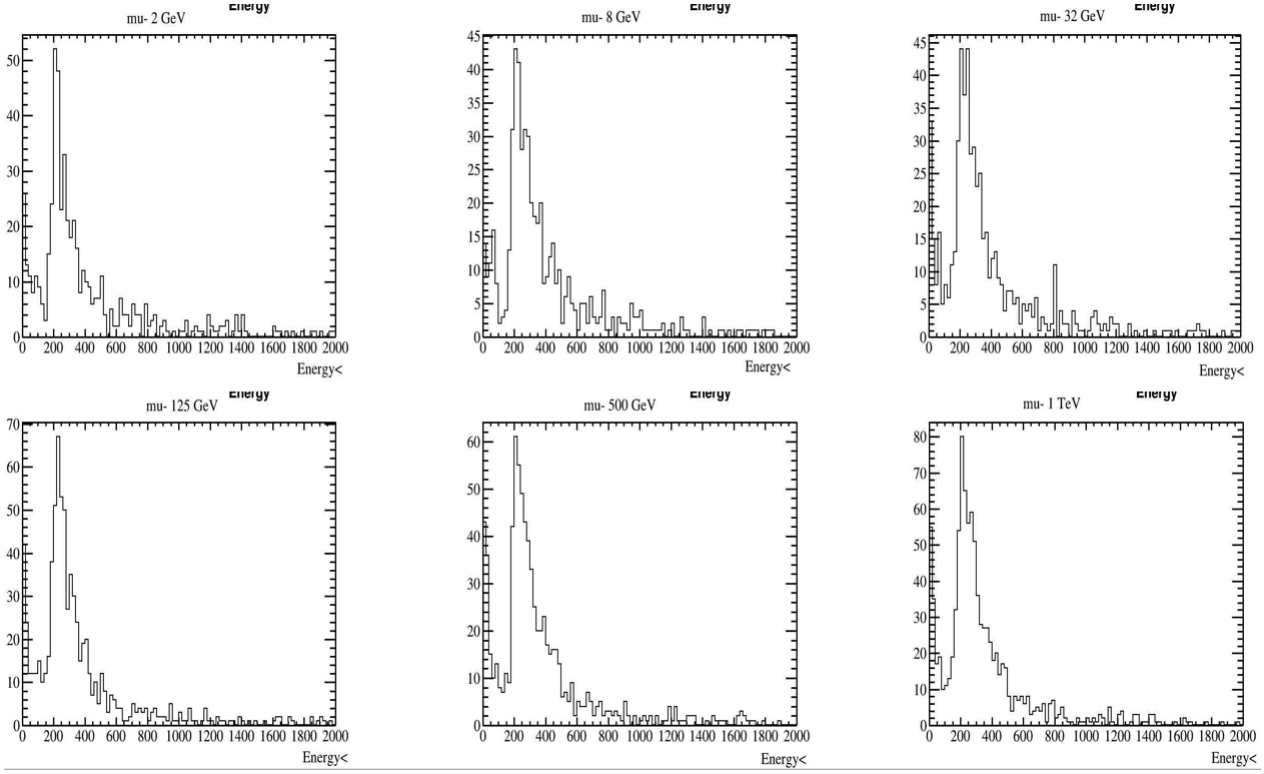

Figure 3.6: Energy deposits profile for muons at different initial kinetic energies. Energies in the histograms are shown in keV.

A way to test this hypothesis is to compare the energy of the cluster with the whole length of the muon tracks. Tacking advantage of the baseball bat shape, we define the cluster length as

$$\sqrt{DX^2 + DY^2 + DZ^2} \tag{3.1}$$

turning DZ into pixels instead of mm. The Z axis elongation is around 50 pixels, as the elongation of the whole CCD in the z-axis is $\frac{670\ \mu m}{15\ \mu m\ per\ pixel} \approx 45$. If the 250 keV peak is related to muons crossing perpendicular to the CCD, there should be a peak in the length histogram, fitting with the energy peak. Indeed, the profile should look very similar, so the muons energy deposits are related to the amount of CCD crossed.

A comparison using a 150000 μ^+ sample is shown in *Figure 3.7*, almost confirming both hypothesis: 250 keV peak is related to muons crossing the whole CCD perpendicular to the x-y plane while the 0 keV peak is related to electrons but not muons.

Also looking at the Geant4 logs, like the ones explained in **Section 2.1.3**, it was found that the particles with very low energy as electrons ripped from the copper surrounding the CCD. This confirms that the 0 keV peak comes from the electrons stripped off the muons passing through.

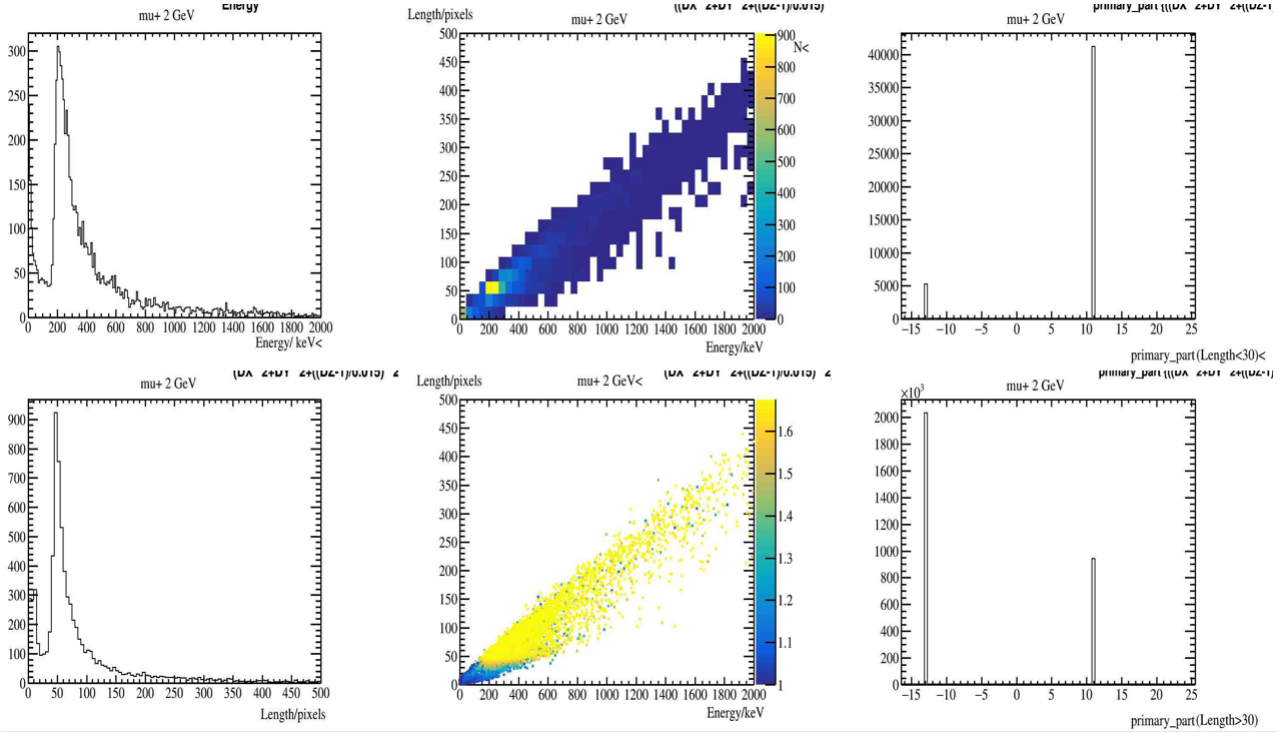

Figure 3.7: Plots for the understanding of the energy peak at 250 keV. Top left: Energy deposit histogram for antimuons with initial kinetic energy 2 GeV. Bottom left: Length of the particle tracks inside the CCD in pixels. Top center: Two first histograms compared in a 2D plot. Color means number of clusters. It can be seen the correlation between the two peaks: the 250 keV one, and the 50 pixels length approximately. Bottom center: Energy deposits versus length with DZ as color. It is shown how the 50 pixels length peak is the point at which the particles start to cross the whole CCD, and below it, they die in few μm. Top right: particle ID of every pixel which cluster has a length below 30 pixels. Most of them are electrons (particle ID=11). Bottom right: particle ID of every pixel which cluster has a length over 30 pixels, being most of them antimuons (particle ID=-13, remembering that antimuon clusters also have electron labeled pixels).

These plots confirmed that muons perpendicular to the CCD leave ≈ a minimum ionizing energy around 250 keV as they cross the full CCDs.

The comparison between a muon and an antimuon does not shown any differences, the typical signature is shown in *Figure 3.8*. The only noticeable difference is the particle leaving the track, and thus they shall not be distinguishable in the experimental data, nor in the machine learning database.

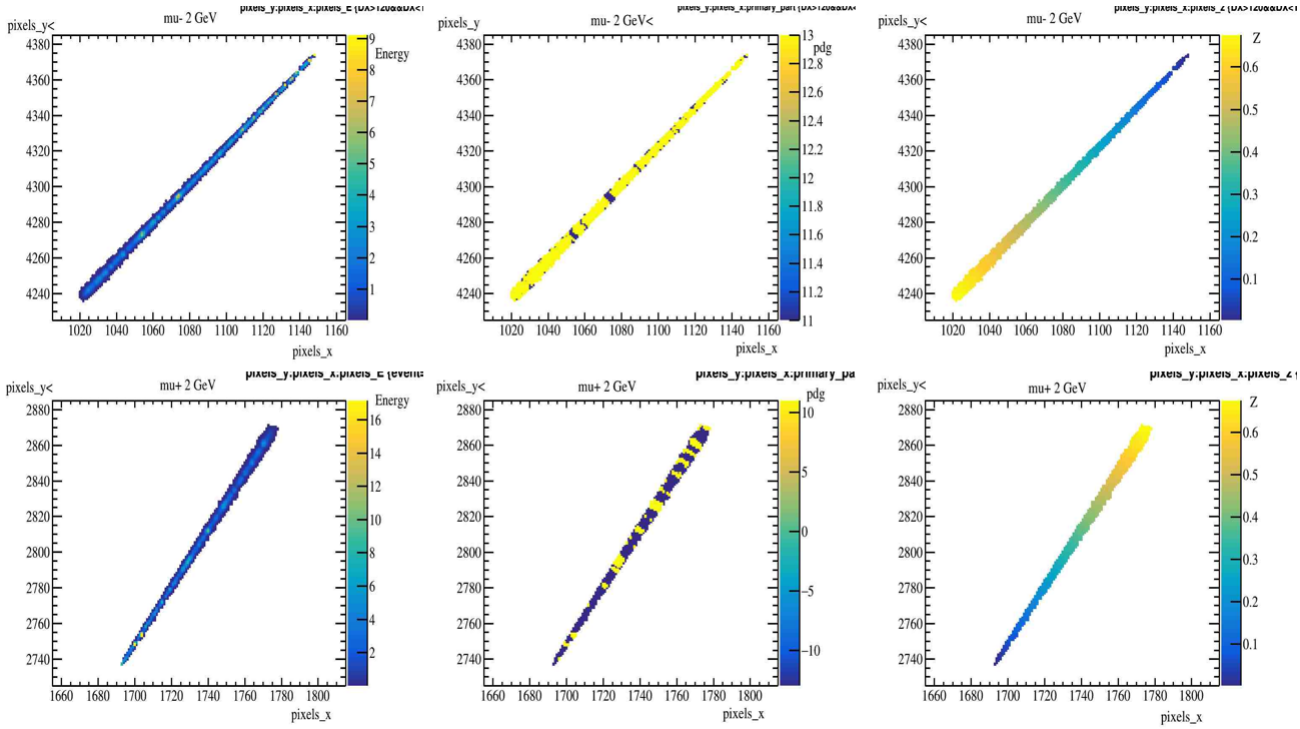

Figure 3.8: 2 GeV muon track as seen in the CCD pixel by pixel, changing the color code information on the three top plots vs same for antimuon on the bottom plots. Left: Track showing energy deposit in each pixel (keV). Center: Track showing which particle leaves the greatest amount of energy in each pixel (Top: 13 (yellow) for muons, 11 (blue) for electrons, while Bottom: 11 (yellow) for electrons, -13 (blue) for antimuons). Right: Track showing the energy deposit's depth within the CCD (mm).

Understanding rare events during muon simulation

During muon analysis, some clusters were found regarding relatively rare secondary processes. These processes are way less expected statistically than the ones explained before, but they need to be further understood as they could be different background signals. They also could serve for the database creation. These are shown in *Figure 3.9*, and explained in the following paragraphs.

Protons were found as a secondary particle (1 proton in 270000 muons simulated) and marked as important because, although they look very similar to muons (as minimum interacting particles), they might be distinguishable by the width of the "baseball bat" shape.

Another rare finding (again 1 out of 270000) is the spallation in Silicon nuclei, appearing He-3 nuclei which are very similar to an alpha (alpha study will be described in the next section), and therefore shall not be considered as different for recognition purposes. Neutrons are also expected in the spallation process, but they were not found during this simulations.

The last one is a more common process known as “delta array” which consists in a muon stripping an electron from the silicon while crossing the CCD and thus leaving a double signature. This last type of tracks should be traced as two different particles by the algorithm.

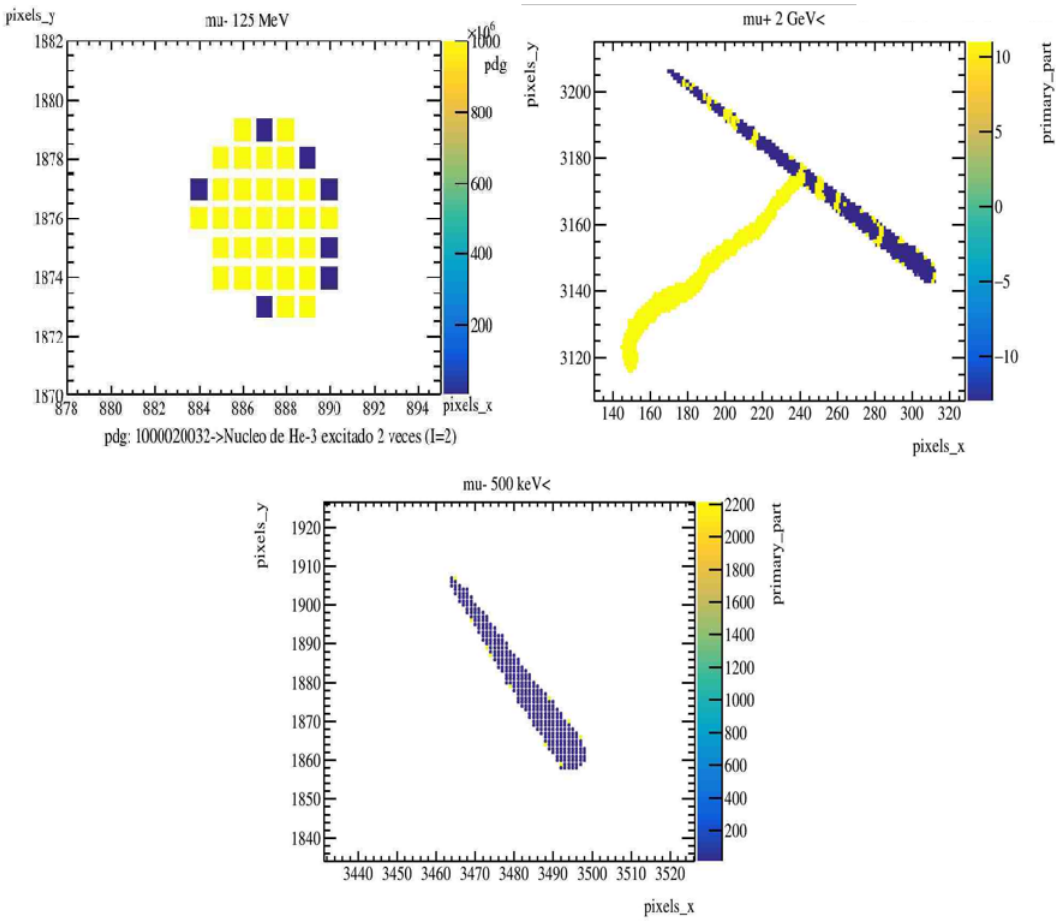

Figure 3.9: Rare cases found during the muon analysis and simulation. Top left: Helium 3 nuclei possibly coming from the activation of silicon with a 125 MeV muon. Top right: Delta array where it can be clearly seen how an antimuon strips an electron from the CCD and the electron leaves its typical bent signature (11 yellow for electrons, -13 blue for antimuons). Bottom: Proton signature, very similar to the ones left by muons, but thicker.

These cases were expected, belong to future work, in a better understanding on protons, neutrons and Helium nuclei behaviour in the CCD, along with delta arrays identification with the machine learning algorithm.

3.2 Alpha analysis

Alphas have also been simulated in order to validate mostly the saturation process, along with the database creation, as stated before in **Section 1.4**. Alpha signatures are a good way to validate the saturation process because of their large energy deposits in a few pixels.

3600 alphas have been simulated from the sensitive detector (CCDSensor) with different energies around the typical alpha kinetic energy (between 4 and 9 MeV due to Geiger-Nuttall law [59]). 300 alpha particles were simulated for each of the following energies: 0.1, 1, 2, 3, 4, 5, 6, 7, 8, 9, 10 and 11 MeV. Alphas are simulated inside the sensitive detector because of their huge stopping power, as they do not travel long distances at the low energy range ($< 9MeV$). Also if they appear in the CCD they are expected from Silicon activation or contaminants inside the CCD, and rarely can come from outside due to its huge mass.

Opposite to muon tracks, alphas are highly dependant on initial kinetic energy because they leave all that initial energy in the initial position. Furthermore, its signature also depends on the initial position, because most of the alphas deposit the energy almost at rest, clusters are highly diffusion dependant: bigger as deeper they are simulated within the silicon bulk of the CCD. Example of alpha clusters at different energies are shown in *Figure 3.10* proving the little changes in shape but big differences in size depending on initial kinetic energy.

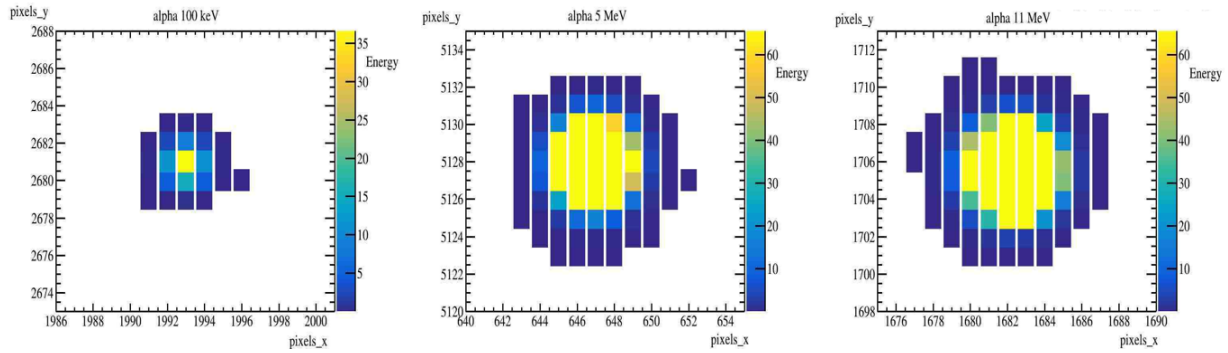

Figure 3.10: Alpha signatures at different energies, drawn pixel by pixel with energy deposit in keV as the color code. Left: 0.1 MeV alpha signature. Center: 5 Mev alpha signature, expected ones from experimental data (typical energy). Right: 11 MeV alpha signature, where alpha movement starts to appear (less circular and more stretched tracks).

Alphas signatures as rounded clusters, and the lost of circularity due to the alphas moving through the silicon at higher energies can be shown in the DX vs DY plot. The most of the alphas should have similar DX and DY distribution, thus DX vs DY plot should be linear, getting broader at higher energies because the alphas have some boost. This is seen in *Figure 3.11*.

The difference in radius size in the alpha signatures is caused by the semiconductor diffusion, the deeper the alphas is the greater the diffusion will be. Therefore it must exist a linear dependence

between the energy deposit Z position, and the signature radius size. This linear dependence is shown in *Figure 3.12*, a fit to the data by the chi squared method has been done. The goodness of the fit is worse with increasing energy of the alpha particles, due to the loss of circularity explained before.

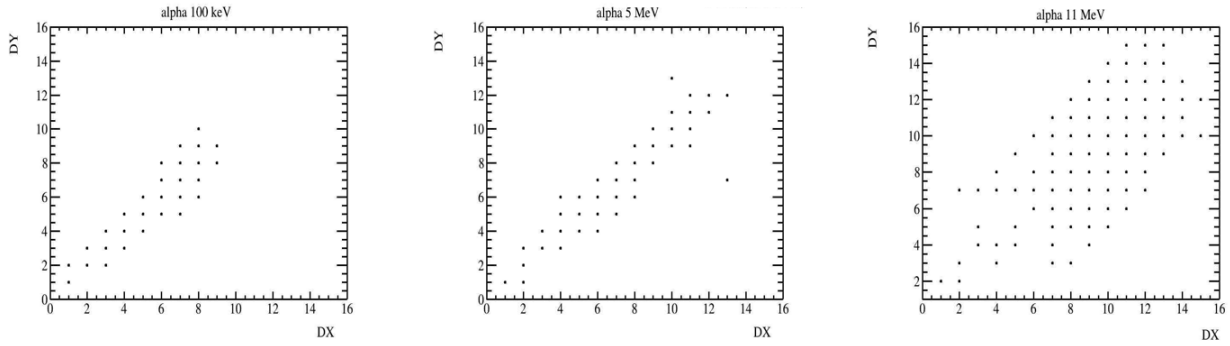

Figure 3.11: Alpha DX vs DY at different energies (both in pixels). The loss of circularity at higher energies can be seen in the right plot, as the plot linearity disperses widely.

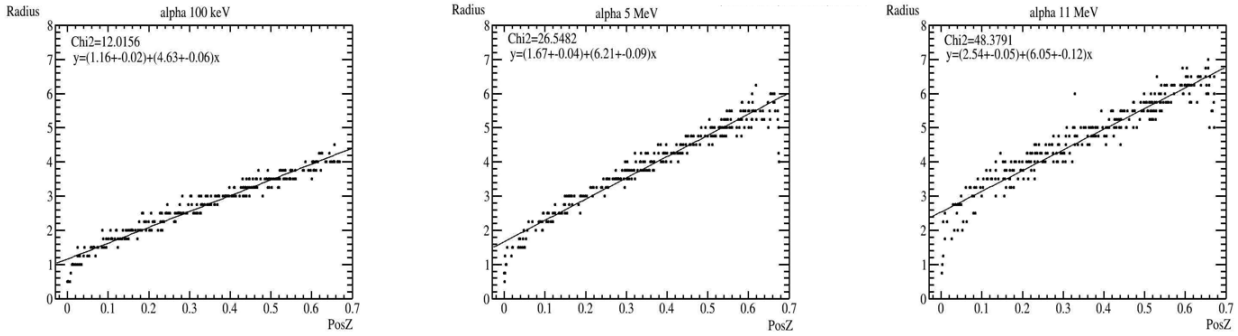

Figure 3.12: Radius of the alpha signatures (pixels) vs Energy deposit position in the Z axis (mm). Radius is calculated as a mean Radius equal to $\frac{DX+DY}{4}$*. As the diffusion in the CCD is energy dependant, the fitted parameters change for different energies.*

Also another way to see the distortion of the round cluster for the high energy alphas due to its boost is looking at cut of the fit with the ordinate axis. Fitting parameters are shown inside the *Figure 3.12* on top left. As expected for low energies they cross at 1, and this crossing increase with energy as expected from the loss of circularity.

Alphas energy deposits do not show much information of the original alpha's energy due to saturation, but explain more about the Gaussian diffusion process. Indeed, the deeper the alpha particle is generated, the lesser pixels are saturated, because due to diffusion, the energy gets distributed between more pixels. This whole energy/saturation analysis is better explained in *Figure 3.13*.

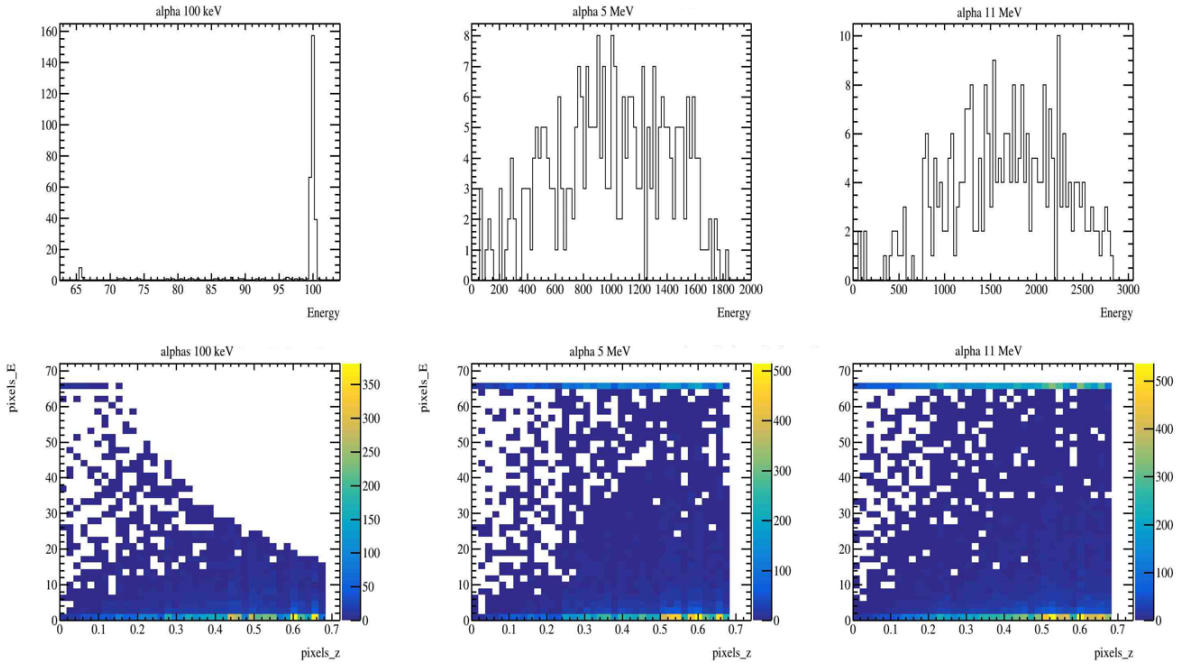

Figure 3.13: Top: Energy deposit per cluster (keV) histogram for different alpha initial kinetic energies. Bottom: Pixel energy vs depth of the energy deposit in said pixels. Saturation was proven miscalculated, as it was expected at 17 keV and was programmed at around 65 keV, but for analysis purposes this is not important and will be corrected for newer versions of psimulCCDimg. The Gaussian curves for the Energy histogram are related to the diffusion process.

As it can be seen, alphas are easier to understand and analyze than muons and other minimum ionizing particles. This allows a fast distinction without needing the machine learning algorithm between minimum ionizing particles and alphas, He-3, and other massive particles by using the already defined "length" of tracks ($\sqrt{DX^2 + DY^2 + DZ^2}$.

The difference between minimum ionizing particles and massive particles such as alphas is logical when using the length of tracks, as alphas do not travel far in the Z axis that part is almost negligible, and track size in the x-y plane is only related to diffusion and not to the movement of the particle, opposite to what happens with muons.

In *Figure 3.14* the difference can be seen clearly. In this figure electrons are not included because for these variables, in most cases, they are not distinguishable from muons; particles perpendicular to the x-y plane tracks look almost the same (mostly rounded), and as the electron bending is smaller than the diffusion, tracks look almost like circles in both cases. That's why the distinction is made between minimum ionizing particles and others, and thus the need of the machine learning algorithm that could distinguish in some cases electrons from muons, for example.

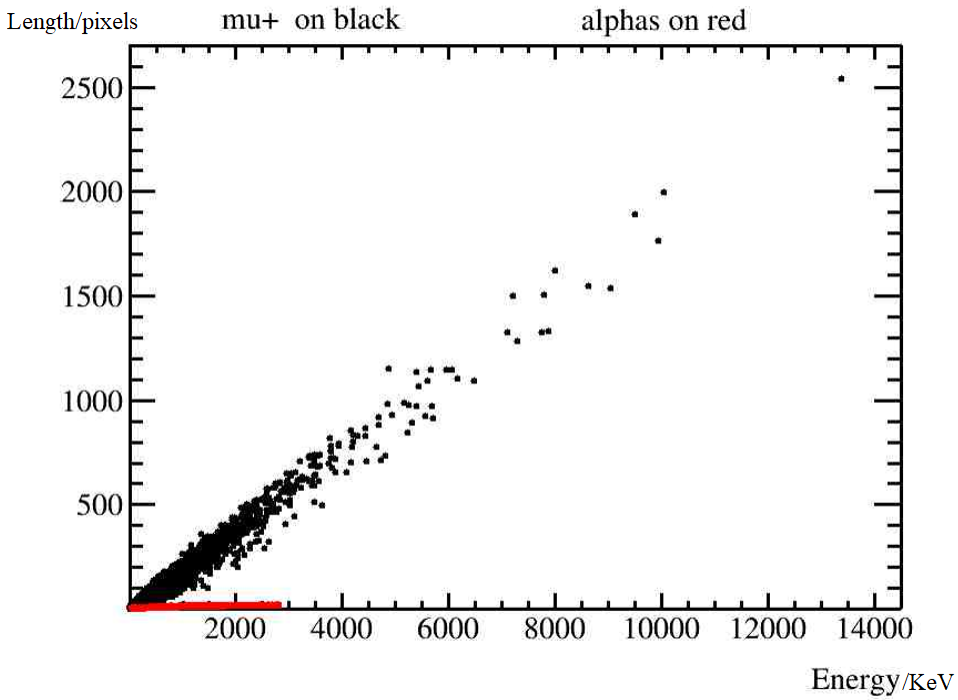

Figure 3.14: Comparison in track lengths between a 150000 μ^+ with initial kinetic energy of 2 GeV sample (black) and a 3600 alpha particles between 0.1 and 11 MeV sample (red). The difference is clear, and can be used as a fast recognition pattern for different particles within the real experimental data.

All in all, alphas are way easier to distinguish than muons because of their large energy deposits.

4 — Conclusion

As seen through this application, alphas and muons have been simulated in order to validate the software used for the direct detection DAMIC-M simulations using the LBC geometry. The flux of muons used for this work do not agree with the muon flux expected at Modane, its reason is mostly for software validation purposes.

Along this work several, both simulation softwares have been tested, changed when necessary and validated.

CCD behaviour for muons and alphas has study in depth to better understood the possible background signals. With this work we have obtained simple methods to differentiate between both particles and those of similar characteristics (minimum ionizing particles vs alpha type particles, massive and highly interacting). Muons are baseball-bat shaped, like protons, but the latter are wider while electrons are bent bats (more worm-like), but when traversing the CCD perpendicular to the x-y plane they appear really similar (like circles).

It has been found how in some cases electrons, muons and protons can not be easily distinguished. That happens when these particles are in the energy region where barely interact with the material (i.e. MIPs). In this cases, alternatives methods, like machine learning algorithm, would be useful to track and classify these type of particles.

In summary: All in all this work has helped in the understanding of the passage of particles through the CCD. It also has led to the improvement of the simulation process, validating and upgrading the simulation software, specially psimulCCDimg, the one used to reconstruct the CCD detection behaviour.

4.1 Future work

As a future research, protons and electrons are yet to be better analysed in the search for a way to distinguish between muons, electrons and protons.

An analysis on cluster distribution homogeneity was started, in order to be able to find sources of inhomogeneity in some particle simulations. This could be useful to trace down contaminants in pieces of the experimental setup, like contaminants coming from cable for example. This is still a work in progress, and will be better defined in the future.

Bibliography

[1] `http://pla.esac.esa.int/pla/`. Release from 2018, last visited 15/03/2020.

[2] J. C. Kapteyn. First Attempt at a Theory of the Arrangement and Motion of the Sidereal System. *The Astrophysical Journal*, 55:302, May 1922.

[3] Heinz Andernach and Fritz Zwicky. English and Spanish Translation of Zwicky's (1933) The Redshift of Extragalactic Nebulae. *arXiv e-prints*, page arXiv:1711.01693, November 2017.

[4] G. R. Burbidge and E. Margaret Burbidge. The Hercules Clusters of Nebulae. *The Astrophysical Journal*, 130:629, September 1959.

[5] Sidney van den Bergh. The Stability of Clusters of Galaxies. *Zeitschrift für Astrophysik*, 55:21, January 1962.

[6] Conference on the Instability of Systems of Galaxies (Santa Barbara, California). *Astronomical Journal*, 66:533, December 1961.

[7] Vera C. Rubin and Jr. Ford, W. Kent. Rotation of the Andromeda Nebula from a Spectroscopic Survey of Emission Regions. *Astrophysical Journal*, 159:379, February 1970.

[8] K. C. Freeman. On the Disks of Spiral and S0 Galaxies. *Astrophysical Journal*, 160:811, June 1970.

[9] `https://hubblesite.org/contents/media/images/2008/32/2402-Image.html?news=true`. Last visited 06/07/2020.

[10] D. H. Rogstad and G. S. Shostak. Gross Properties of Five Scd Galaxies as Determined from 21-Centimeter Observations. *Astrophysical Journal*, 176:315, September 1972.

[11] Jeremy L. Tinker, Brant E. Robertson, Andrey V. Kravtsov, Anatoly Klypin, Michael S. Warren, Gustavo Yepes, and Stefan Gottlöber. The large-scale bias of dark matter halos: Numerical calibration and model tests. *The Astrophysical Journal*, 724(2):878–886, Nov 2010.

[12] E. Komatsu, J. Dunkley, M. R. Nolta, C. L. Bennett, et al. Five-Year Wilkinson Microwave Anisotropy Probe Observations: Cosmological Interpretation. *The Astrophysical Journal Supplement*, 180(2):330–376, February 2009.

[13] Jacob D. Bekenstein. Alternatives to dark matter: Modified gravity as an alternative to dark matter, 2010.

[14] Carl H. Gibson. Fluid mechanics explains cosmology, dark matter, dark energy, and life, 2012.

[15] Sebastian Baum, Katherine Freese, and Chris Kelso. Dark matter implications of dama/libra-phase2 results. *Physics Letters B*, 789:262 – 269, 2019.

[16] Giulia D'Imperio. Dark matter search with the sabre experiment, 2018.

[17] D.S. Akerib, S. Alsum, H.M. Araújo, X. Bai, A.J. Bailey, J. Balajthy, P. Beltrame, E.P. Bernard, A. Bernstein, T.P. Biesiadzinski, and et al. Results from a search for dark matter in the complete lux exposure. *Physical Review Letters*, 118(2), Jan 2017.

[18] Xiangyi Cui, Abdusalam Abdukerim, Wei Chen, Xun Chen, Yunhua Chen, Binbin Dong, Deqing Fang, Changbo Fu, Karl Giboni, Franco Giuliani, and et al. Dark matter results from 54-ton-day exposure of pandax-ii experiment. *Physical Review Letters*, 119(18), Oct 2017.

[19] E. Aprile, J. Aalbers, F. Agostini, M. Alfonsi, L. Althueser, F.D. Amaro, M. Anthony, F. Arneodo, L. Baudis, B. Bauermeister, and et al. Dark matter search results from a one ton-year exposure of xenon1t. *Physical Review Letters*, 121(11), Sep 2018.

[20] C. Amole, M. Ardid, I.J. Arnquist, D.M. Asner, D. Baxter, E. Behnke, M. Bressler, B. Broerman, G. Cao, C.J. Chen, and et al. Dark matter search results from the complete exposure of the pico-60 c3f8 bubble chamber. *Physical Review D*, 100(2), Jul 2019.

[21] R. Agnese, A.J. Anderson, M. Asai, D. Balakishiyeva, R. Basu Thakur, D.A. Bauer, J. Beaty, J. Billard, A. Borgland, M.A. Bowles, and et al. Search for low-mass weakly interacting massive particles with supercdms. *Physical Review Letters*, 112(24), Jun 2014.

[22] G. Angloher, A. Bento, C. Bucci, L. Canonica, X. Defay, A. Erb, F. von Feilitzsch, N. Ferreiro Iachellini, P. Gorla, A. Gütlein, and et al. Results on light dark matter particles with a low-threshold cresst-ii detector. *The European Physical Journal C*, 76(1), Jan 2016.

[23] Alvaro Chavarria, Javier Tiffenberg, et al. Damic at snolab, 2014.

[24] J. Angle, E. Aprile, F. Arneodo, L. Baudis, A. Bernstein, A. Bolozdynya, P. Brusov, L. C. C. Coelho, C. E. Dahl, L. DeViveiros, and et al. First results from the xenon10 dark matter experiment at the gran sasso national laboratory. *Physical Review Letters*, 100(2), Jan 2008.

[25] P. Agnes, I.F.M. Albuquerque, T. Alexander, A.K. Alton, G.R. Araujo, M. Ave, H.O. Back, B. Baldin, G. Batignani, K. Biery, and et al. Darkside-50 532-day dark matter search with low-radioactivity argon. *Physical Review D*, 98(10), Nov 2018.

[26] T. Aralis, T. Aramaki, I.J. Arnquist, E. Azadbakht, W. Baker, S. Banik, D. Barker, C. Bathurst, D.A. Bauer, L.V.S. Bezerra, and et al. Constraints on dark photons and axionlike particles from the supercdms soudan experiment. *Physical Review D*, 101(5), Mar 2020.

[27] M Boezio, M Pearce, et al. PAMELA and indirect dark matter searches. *New Journal of Physics*, 11(10):105023, oct 2009.

[28] R. Caputo, M. R. Buckley, P. Martin, E. Charles, A. M. Brooks, A. Drlica-Wagner, J. Gaskins, and M. Wood. Search for gamma-ray emission from dark matter annihilation in the small magellanic cloud with the fermi large area telescope. *Phys. Rev. D*, 93:062004, Mar 2016.

[29] S. J. Asztalos, G. Carosi, C. Hagmann, D. Kinion, K. van Bibber, M. Hotz, L. J Rosenberg, G. Rybka, J. Hoskins, J. Hwang, and et al. Squid-based microwave cavity search for dark-matter axions. *Physical Review Letters*, 104(4), Jan 2010.

[30] E. Aprile and others (XENON Collaboration). Dark Matter Results from 225 Live Days of XENON100 Data. *Phys. Rev. Lett.*, 109(18):181301, November 2012.

[31] Daniel Abercrombie, Nural Akchurin, et al. Dark matter benchmark models for early lhc run-2 searches: Report of the atlas/cms dark matter forum. *Physics of the Dark Universe*, 27:100371, 2020.

[32] N. Castelló-Mor. Damic-m experiment: Thick, silicon ccds to search for light dark matter. *Nuclear Instruments and Methods in Physics Research Section A: Accelerators, Spectrometers, Detectors and Associated Equipment*, 958:162933, Apr 2020.

[33] Torsten Åkesson, Asher Berlin, Nikita Blinov, Owen Colegrove, Giulia Collura, Valentina Dutta, Bertrand Echenard, Joshua Hiltbrand, David G. Hitlin, Joseph Incandela, John Jaros, Robert Johnson, Gordan Krnjaic, Jeremiah Mans, Takashi Maruyama, Jeremy McCormick, Omar Moreno, Timothy Nelson, Gavin Niendorf, Reese Petersen, Ruth Pöttgen, Philip Schuster, Natalia Toro, Nhan Tran, and Andrew Whitbeck. Light dark matter experiment (ldmx), 2018.

[34] A. Drukier and L. Stodolsky. Principles and applications of a neutral-current detector for neutrino physics and astronomy. *Phys. Rev. D*, 30:2295–2309, Dec 1984.

[35] Mark W. Goodman and Edward Witten. Detectability of certain dark-matter candidates. *Phys. Rev. D*, 31:3059–3063, Jun 1985.

[36] Teresa Marrodán Undagoitia and Ludwig Rauch. Dark matter direct-detection experiments. *Journal of Physics G: Nuclear and Particle Physics*, 43(1):013001, Dec 2015.

[37] Michael Crisler, Rouven Essig, Juan Estrada, Guillermo Fernandez, Javier Tiffenberg, Miguel Sofo Haro, Tomer Volansky, and Tien-Tien Yu. Sensei: First direct-detection constraints on sub-gev dark matter from a surface run. *Physical Review Letters*, 121(6), Aug 2018.

[38] J. Amaré, S. Cebrián, I. Coarasa, C. Cuesta, E. García, M. Martínez, M.A. Oliván, Y. Ortigoza, A. Ortiz de Solórzano, J. Puimedón, and et al. First results on dark matter annual modulation from the anais-112 experiment. *Physical Review Letters*, 123(3), Jul 2019.

[39] R. Ajaj, P.-A. Amaudruz, G.R. Araujo, M. Baldwin, M. Batygov, B. Beltran, C.E. Bina, J. Bonatt, M.G. Boulay, B. Broerman, and et al. Search for dark matter with a 231-day exposure of liquid argon using deap-3600 at snolab. *Physical Review D*, 100(2), Jul 2019.

[40] The Dark Energy Survey Collaboration. The dark energy survey, 2005.

[41] B. Flaugher et al. The Dark Energy Camera. *The Astronomical Journal*, 150(5):150, November 2015.

[42] A. Aguilar-Arevalo, D. Amidei, and others (DAMIC Collaboration). First direct-detection constraints on ev-scale hidden-photon dark matter with damic at snolab. *Phys. Rev. Lett.*, 118:141803, Apr 2017.

[43] A. Aguilar-Arevalo, D. Amidei, D. Baxter, G. Cancelo, B.A. Cervantes Vergara, A.E. Chavarria, E. Darragh-Ford, J.R.T. de Mello Neto, J.C. D'Olivo, J. Estrada, and et al. Constraints on light dark matter particles interacting with electrons from damic at snolab. *Physical Review Letters*, 123(18), Oct 2019.

[44] S.J. Lee, B. Kilminster, and A. Macchiolo. Dark matter in ccds at modane (damic-m): a silicon detector apparatus searching for low-energy physics processes. *Journal of Instrumentation*, 15(02):C02050–C02050, Feb 2020.

[45] C. J. Bebek, R. A. Coles, et al. CCD research and development at Lawrence Berkeley National Laboratory. In Andrew D. Holland and James W. Beletic, editors, *High Energy, Optical, and Infrared Detectors for Astronomy V*, volume 8453, pages 27 – 42. International Society for Optics and Photonics, SPIE, 2012.

[46] Javier Tiffenberg, Miguel Sofo-Haro, and other. Single-electron and single-photon sensitivity with a silicon skipper ccd. *Phys. Rev. Lett.*, 119:131802, Sep 2017.

[47] S. Agostinelli, J. Allison, and others (Geant4 Collaboration). Geant4—a simulation toolkit. *Nuclear Instruments and Methods in Physics Research Section A: Accelerators, Spectrometers, Detectors and Associated Equipment*, 506(3):250–303, 2003.

[48] `http://ncastell.web.cern.ch/ncastell/getting_started.html`. pysimdamicm documentation, last visited 08/07/2020.

[49] `https://root.cern/doc/master/index.html`. ROOT documentation, last visited 08/07/2020.

[50] R Brun, R Hagelberg, M Hansroul, and J C Lassalle. *Simulation program for particle physics experiments, GEANT: user guide and reference manual.* CERN, Geneva, 1978.

[51] `https://geant4.web.cern.ch/collaboration`. Last visited 10/06/2020.

[52] Gordon R. Hopkinson. Analytic Modeling Of Charge Diffusion In Charge-Coupled-Device Imagers. *Optical Engineering*, 26(8):766 – 772, 1987.

[53] D. Groom, P. Eberhard, Stephen Holland, Michael Levi, N. Palaio, S Perlmutter, R. Stover, and M Wei. Point-spread function in depleted and partially depleted ccds. *LBNL-45276 Optical detectors for Astronomy*, 252, October 1999.

[54] Stephen Holland, Donald Groom, Nick Palaio, Richard Stover, and Mingzhi Wei. Fully depleted, back-illuminated charge-coupled devices fabricated on high-resistivity silicon. *LBNL-49992: Draft for IEEE Transactions on electron devices*, 50(1):225–238, 1 2003.

[55] The DAMIC Collaboration, Alexis A. Aguilar-Arevalo, Xavier Bertou, Melissa J. Butner, Gustavo Cancelo, Alvaro Chavarria, Juan Carlos D'Olivo, Juan Cruz Estrada Vigil, Guillermo Fernandez Moroni, Federico Izraelevitch, Ben Kilminster, Ian T. Lawson, Fernando Marsal, Jorge Molina, Paolo Privitera, Tom Schwarz, Miguel Sofo Haro, Javier Tiffenberg, Frederic Trillaud, and Jing Zhou. Damic: a novel dark matter experiment, 2013.

[56] J. Estrada, J. Molina, J.J. Blostein, and G. Fernández. Plasma effect in silicon charge coupled devices (ccds). *Nuclear Instruments and Methods in Physics Research Section A: Accelerators, Spectrometers, Detectors and Associated Equipment*, 665:90 – 93, 2011.

[57] Donald E. Groom, Nikolai V. Mokhov, and Sergei I. Striganov. Muon stopping power and range tables 10 mev–100 tev. *Atomic Data and Nuclear Data Tables*, 78(2):183 – 356, 2001.

[58] M. Tanabashi et al. Review of Particle Physics. *Phys. Rev. D*, 98(3):030001, 2018.

[59] H. Geiger Ph.D. and J.M. Nuttall B.Sc. Lvii. the ranges of the alpha particles from various radioactive substances and a relation between range and period of transformation. *The London, Edinburgh, and Dublin Philosophical Magazine and Journal of Science*, 22(130):613–621, 1911.

5 — Appendix I: macros and their creation script

In this appendix a macro file for Geant4 will be shown as an example along with the Python script written for creating them.

A macro file is a text file with a sequence of commands used by Geant4 to run a simulation. In the case shown in this Appendix, the macro file is used to simulate a ^{60}Co isotope in the sensitive detector volume of the LBC geometry (called internally CCDSensor_PV). Let's start by showing the whole macro file:

```
/control/verbose 1
/run/verbose 1
/run/initialize
/tracking/verbose 1
/event/verbose 1
/random/setSeeds 712  1789
/damic/gun/particle ion
/damic/gun/ion 27 60 0 0.0
/damic/gun/energy/mono 0 eV
/damic/gun/direction/oned
/damic/gun/direction/onedX 1
/damic/gun/direction/onedY 0
/damic/gun/direction/onedZ 0
/damic/gun/position/dovolume
/damic/gun/position/addvolume CCDSensor_PV 1
/analysis/setFileName CCDSensor_PV_60a27z_N1
/run/beamOn 1
```

The first five lines include the initialize and verbose commands. Verbose is used to regulate the output information given by Geant4. Verbose 0 implies no information given about the tracked particles, or the internal processes for example. In this case there is an interest in that information as it is wanted to know the processes the Cobalt undergoes. The initialize command, obviously starts the simulation. The /random/setSeeds command uses two numbers as a record for the random position of the particle. It is used in case there is a need to "re-simulate" a particle in the same initial conditions.

The /damic/gun/ class allows to set the particle properties such as type of particle (ion), initial kinetic energy (0 eV), direction (mandatory even when the initial kinetic energy is null), or initial volume (CCDSensor in this case). The /run/beamOn command sets the number of particles simulated.

This is just an example macro, but the same files are used to simulate radioisotopes, particles such an electrons or alphas, etc. A Python script was written by Núria Castelló-Mor for writing this macros automatically for radioisotopes by giving the initial volume, the atomic and mass number, the number of particles to simulate, etc. This script was adapted to create macros for individual particles (electron, alphas, muons, etc) by giving the particle name, initial volume and initial kinetic energy to make writing these macros much easier. The code is given ahead (the red arrows are used to emphasize a line break not included in the original code):

```
#!/usr/bin/env python3
"""":script:‘createMacros4G4Sims‘
       It produces the macros to run Geant4 simulations (DAMICG4_Sims) of DAMIC-M
           ↪ Experiment

"""

headLinesList = ["/control/verbose␣0","/run/verbose␣0","/run/initialize","/
    ↪ tracking/verbose␣0",
       "/event/verbose␣0","/random/setSeeds␣seed1␣␣seed2","/damic/gun/particle␣
           ↪ particlename"]
headLines = "\n".join(headLinesList)

ionLinesList = ["\n/damic/gun/energy/mono␣Ekin␣eV","/damic/gun/direction/distri␣
    ↪ Isotropic","/damic/gun/direction/thetamin␣0",
       "/damic/gun/direction/thetamax␣180","/damic/gun/direction/phimin␣-180","/
           ↪ damic/gun/direction/phimax␣180"]
ionLines = "\n".join(ionLinesList)

dovolLinesList = ["/damic/gun/position/dovolume","/damic/gun/position/addvolume␣
    ↪ pvname"]
dovolLines = "\n".join(dovolLinesList)

dosurfLineList =["/damic/gun/position/dosurface",
    "/damic/gun/position/setadvdiffmodel␣true",
    "/damic/gun/position/setminembeddist␣Dmin␣Dunit","/damic/gun/position/
        ↪ setmaxembeddist␣Dmax␣Dunit",
    "/damic/gun/position/addvolume␣pvname"]
dosurfLines = "\n".join(dosurfLineList)
```

```
saveLinesList = ["/analysis/setFileName␣saveas", "/run/beamOn␣NbeamOn"]
saveLines = "\n".join(saveLinesList)



def DoMacro( isDoVolume, kind, saveas, particlename, pvname, NbeamOn, seeds
    ↪ =[321,4321],
        multiplicity=False, pv_start=0, pv_end=0, pv_step=1,
        Dunit="nm", Dmin=0.0,Dmax=100.0, Ekin=0.0, add_PV=False):
    """
    Create the macro file to simulated the induced spectral background due to
        ↪ contaminants on the
    the physical volume <pvname>.


    Parameters
    ----------

    isDoVolume : bool
            set if the primary particle must be randomly placed on the bulk of the
                ↪ <pvname>;
            unset if it must be placed only on the <pvname> surface

    kind : int
            an ID to identify the output ROOT file of the G4sims which follows the
                ↪ patter
                <pvname>_<particlename>_<Ekin>eV_N<NbeamOn>.mac

    saveas : string
            output macro file name

    particlename: string
            name of the particle you want to simulate (eg: alpha, e-, mu-)

    pvname : string
            physical volume name where primaries will be pseudo-randomly placed (at
                ↪  is appear on the GDML file)

    NbeamOn : int
            number of primary particels that you want to simulate

    Ekin : float
            kinetic energy of the simulated particle
```

```
seeds : array_like
        two integers to set the seeds of the pseudo-random generation algorithm


multiplicity : bool
        to allow simulations for a given physical volume family (assuming a
            ↪ pattern name string
        like <pvname>_ID_PV )

pv_start : int
        first ID of the physical volume family's name (assuming a pattern name
            ↪ string like
        <pvname>_ID_PV)

pv_end : int
        end ID of the the physical volume family's name

pv_step : int
        step to go from the first up to the end ID


Dunit : string
        unit of the depth (Dmin and Dmax) to embed particle generated on the
            ↪ surface of the
        volume <pvname>

Dmin : float
        minimum depth to embed particles generated on the surface of the volume
            ↪  <pvname>

Dmax : float
        maximum depth to embed particles generated on the surface of the volume
            ↪  <pvname>


Examples
--------

Let's assume you generated 3 independet (seed) macro files to randomly place <
    ↪ NbeamOn> times
the particle (electron, for example) on volume CCDSensor (surface or bulk) to
    ↪ get the traces.
```

```
user$ create_macros_for_DB -p e- --NbeamOn 1000 --Emin 50 --Emax 150 -v
    ↪ CCDSensor_PV -o test --dE 10


This will create 11 macro files with varying energies between 50 and 150 eV on
    ↪  10 eV steps, with a thousand electrons each.
Each macro will be called test_ID, with ID going from 0 to 10 included.


"""

if isDoVolume:
    VolLines = dovolLines
else:
    VolLines = dosurfLines
    VolLines = VolLines.replace("Dunit",Dunit)
    VolLines = VolLines.replace("Dmin",str(Dmin))
    VolLines = VolLines.replace("Dmax",str(Dmax))

macroLines = headLines.replace("seed1", str(seeds[0])).replace("seed2", str(
    ↪ seeds[1]))
macroLines = macroLines.replace("particlename",str(particlename))
macroLines += ionLines+"\n"
macroLines = macroLines.replace("Ekin",str(Ekin))


if multiplicity:
    macroLines += VolLines.replace("pvname", "␣{0}␣1␣true␣{1}␣{2}␣{3}\n".
        ↪ format(pvname,
        pv_start,pv_end,pv_step) )
else:
    if add_PV:
        macroLines += VolLines.replace("pvname","{0}_PV␣1\n".format(pvname))
    else:
        macroLines += VolLines.replace("pvname","{0}␣1\n".format(pvname))

outroot = "{0}_{1}_{2}eV_N{3}".format(pvname,particlename,str(int(Ekin)),
    ↪ NbeamOn)

macroLines += saveLines.replace("saveas",outroot).replace("NbeamOn",str(
    ↪ NbeamOn))

fout = open( saveas, "w+")
fout.writelines( macroLines )
```

```
    fout.close()
    return

##################################################

if __name__ == '__main__':

    import argparse
    import os
    import pandas as pd
    import numpy as np

    parser = argparse.ArgumentParser()

    parser.add_argument("-p",
           action='store',
           dest='particlename',
           help="name␣of␣the␣particle␣to␣simulate"
           )

    parser.add_argument("--NbeamOn",
           action='store',
           dest='NbeamOn',
           type=int,
           default=100,
           help="number␣of␣particles␣simulated␣on␣each␣macro"
           )

    parser.add_argument("--Emin",
           action='store',
           dest='Emin',
           type=float,
           default=0,
           help="minimum␣energy␣for␣the␣simulated␣particles␣on␣eV"
           )

    parser.add_argument("--Emax",
           action='store',
           dest='Emax',
           type=float,
           help="maximum␣energy␣for␣the␣simulated␣particles␣on␣eV"
           )

    parser.add_argument("-v",
```

```
        action='store',
        dest="pvname",
        type=str,
        help="physical␣volume␣name␣as␣it␣appears␣in␣the␣GDML␣geometry␣file"
        )

parser.add_argument("-m",
        action='store',
        dest='multiplicity',
        nargs="+",
        type=int,
        default=[0,1,1,1],
        help="set␣to␣1␣to␣add␣several␣volumes,␣three␣extra␣arguments␣must␣be␣
            ↪ informed,␣min,␣max␣and␣stepping␣values␣for␣the␣ID␣volume␣number␣
            ↪ "
        )

parser.add_argument("--in-surface",
        action='store_false',
        dest="dovolume",
        help="Use␣if␣simulated␣isotopes␣must␣be␣placed␣only␣on␣the␣surface␣of␣
            ↪ the␣simulated␣volume,␣-v"
        )

parser.add_argument("-o",
        action='store',
        dest="saveas",
        type=str,
        help="macro␣output␣file␣name,␣which␣follows␣the␣specific␣pattern␣name␣<
            ↪ saveas>_<index>.mac␣␣"
        )

parser.add_argument("--dE",
        action='store',
        dest="dE",
        type=int,
        default=0,
        help="Energy␣difference␣between␣macros␣(needed␣if␣-n␣is␣not␣used)"
        )

parser.add_argument("-n",
        action='store',
        dest="N",
        type=int,
```

```
        help="number␣of␣macros␣created␣(needed␣if␣the␣maximum␣energy␣is␣not␣
            ↪ given).␣The␣output␣file␣name␣is␣<saveas>_n.mac␣"
        )

parser.add_argument("--noffset",
        action='store',
        dest="noffset",
        type=int,
        default=0,
        help="offset␣in␣the␣n␣value␣for␣each␣generated␣macro,␣i.e.␣<saveas>_n+
            ↪ noffset.mac"
        )

parser.add_argument("-s","--seeds",
        action='store',
        dest="seeds",
        nargs="+",
        type=int,
        default=[321,4321],
        help="two␣integers␣to␣set␣the␣seeds␣of␣the␣pseudo-random␣generation␣
            ↪ algorithm"
        )


arg = parser.parse_args()

if arg.saveas is None:
    raise Exception("\n\nArgumentError.␣The␣option␣-o␣is␣mandatory\n\n")

if arg.pvname is None:
    raise Exception("\n\nArgumentError.␣The␣option␣-v␣is␣mandatory\n\n")

if arg.Emax is None:
    Emax=arg.Emin
else:
    Emax=arg.Emax

if arg.multiplicity[0] == 0:
    multiplicity = False
else:
    multiplicity = True

_,pv_start,pv_end,pv_step = arg.multiplicity
```

```
if arg.N is None:
    if Emax<arg.Emin:
        raise Exception("\n\nArgumentError. The maximum energy is lesser than
            ↪ the minimum one.\n\n")

    n_macros=1+int((Emax-arg.Emin)/arg.dE)

else:
    n_macros=arg.N

dseed = 0
for i in range(n_macros):
    seeds = np.array(arg.seeds) + dseed
    saveas = arg.saveas+"_{0}.mac".format(i+arg.noffset)
    Ekin = arg.Emin + i*arg.dE
    DoMacro(arg.dovolume, i+1+arg.noffset, saveas, arg.particlename, arg.
        ↪ pvname, arg.NbeamOn, seeds=seeds, multiplicity=multiplicity,
        ↪ pv_start=pv_start, pv_end=pv_end, pv_step=pv_step, Ekin=Ekin)
    dseed+=100
    print("macro for particle {0} saved as {1}".format(arg.particlename,saveas
        ↪ ))


msm = """
macro files are done!


"""
print(msm)
```